Journal of Thermoplastic Composite Materials

http://jtc.sagepub.com

Modeling of Heat Transfer and Crystallization in Thermoplastic Composite Tape Placement Process

Fazil O. Sonmez and H. Thomas Hahn

Journal of Thermoplastic Composite Materials 1997; 10; 198
DOI: 10.1177/089270579701000301

The online version of this article can be found at:
http://jtc.sagepub.com/cgi/content/abstract/10/3/198

Published by:
SAGE Publications
http://www.sagepublications.com

Modeling of Heat Transfer and Crystallization in Thermoplastic Composite Tape Placement Process

FAZIL O. SONMEZ AND H. THOMAS HAHN*
Mechanical, Aerospace and Nuclear Engineering Department
University of California
Los Angeles, CA 90024

ABSTRACT: The crystallization behavior of thermoplastic composites during the tape placement process has been analyzed. A heat transfer analysis has been carried out using a finite element method. The heat transfer analysis is coupled with a crystallization kinetics model to predict the resulting morphology. In order to determine the heat intensity that could be applied to the laminate, a degradation kinetics model is added. The degradation kinetics model thus provides an upper bound for the heat input. The models relate the process parameters (e.g., roller velocity, roller pressure, heat input) to temperature and crystallinity distributions and degradation weight loss. These models are incorporated into a computer code to generate numerical results. By using this code, process conditions which are favorable to consolidation and also likely to produce optimum crystallinity levels are identified.

1. INTRODUCTION

DURING PROCESSING, THERMOPLASTIC composites undergo a number of microstructural changes that affect their subsequent properties. These changes include melting, crystallization, development of residual strains, degradation, void formation, and consolidation. All of these are strongly affected by the process temperature history. Understanding these changes and being able to predict them are essential to ensuring the quality of fabricated parts.

A number of numerical and analytical models have been used to describe heat transfer in the processing of thermoplastic composites. One of the simple cases was heat transfer in the press molding process, where a composite laminate was melted in an oven and then transferred to a mold to be cooled down [1–4]. The main goal was to determine the resulting cooling rates and crystallinity levels.

*Author to whom correspondence should be addressed.

0892-7057/97/03 0198–43 $10.00/0

Blundell and Willmouth [3] found that cooling rates through the crystallization zone (320°C–180°C for polyetheretherketone) were approximately the same across the whole thickness of the laminate unless the laminate was too thick. If the mold was at room temperature and made of a highly conductive material, the resulting laminate would have an amorphous surface and a crystalline interior. Saliba et al. [5] extended the analysis to more complex shapes and investigated transient heat transfer by using a finite difference method. Maffezzoli et al. [6,7] and later Xiao et al. [8] developed heat transfer models for resistance welding of composite parts, where resistive heating was used to melt the matrix by passing an electric current through the carbon fibers. Astrom and Pipes [10] carried out a heat transfer analysis of the thermoplastic pultrusion process.

In the thermoplastic tape-placement process, an incoming composite tape is bonded to a previously laid and consolidated laminate under heat, and pressure is applied locally to the interface (Figure 1). Various tape product forms are commercially available. Reinforcing (carbon or glass) fibers could be commingled or co-woven with thermoplastic fibers. They could also be preimpregnated or coated with a thermoplastic resin. Consolidation is achieved by squeezing out the entrapped air under the pressure of a compaction shoe or roller and allowing interlaminar molecular diffusion of polymer chains to take place. By laying additional layers in different directions, a part with the desired thickness and properties can be fabricated. Filament winding is a special case of the tape-placement process, in which a tape is wound on a rotating cylindrical mandel to form the part.

A number of heat transfer models have been proposed for the tape-placement [9–16] and filament-winding process [17–19]. Güçeri and his coworker [9,12,19] used a finite difference method to show that very high temperature gradients existed near the nip point, and the roller velocity, heat input and preheating significantly affected the temperature field within the laminate.

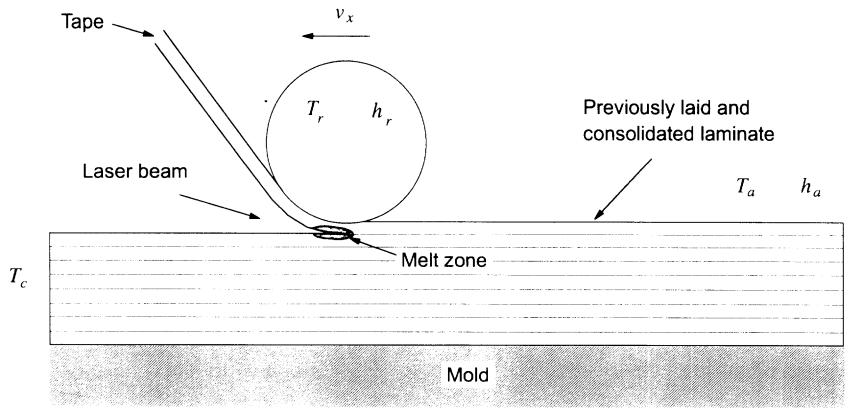

Figure 1. *General configuration of the thermoplastic tape-placement process.*

Several experimental studies also attempted to identify the main processing parameters and their effects on tape placement [20–26] and filament winding [27–46]. Processing at high tempertures and pressure was found to reduce void content [30,35,43]. Anderson and Colton [22] recommended preheating of the laminate, while Astrom and Pipes [31] recommended cooling of the roller to avoid sticking of the resin. Since different experimental setups, materials, and heat sources were used, no universal conclusions could be drawn. Nevertheless, the overriding problem encountered in those experiments was either thermal degradation of the matrix due to excessive heat intensity or high void content due to incomplete consolidation. It was difficult to find a processing window to achieve a compromise between these two conflicting requirements. Consolidation of the tape has been achieved at laydown rates slower than 1.5 cm/s. These consolidation speeds are below the desired values for commercial applications. Also, void contents as low as 1% are required by the industry [47]. Higher production rates could be achieved if the correct combination of processing parameters was applied. Previous studies show that a thorough understanding of the effects of the processing parameters is needed in order to use the tape-placement process as a viable manufacturing method.

In order to achieve good consolidation, the tape-laminate interface temperature should be above the melting temperature (345°C for PEEK). For molding, the prepreg manufacturer's recommended processing temperature range for APC-2 is 370–390°C [48], and the minimum processing temperature is reported to be 360°C [49]. However, due to relatively short consolidation times with the tape-placement process, the interface should be raised to higher temperatures to take advantage of lower viscosities and to ensure complete melting of crystallites. It should also be noted that when a polymer is exposed to high temperatures, it tends to degrade and decompose due to the unstable or reactive condition of covalent bonds. The thermal degradation behavior of PEEK has been extensively studied [50–58]. PEEK shows exceptional thermal stabilities, exhibiting only minimal weight loss up to 500°C when heated in air or nitrogen at 10°C/min [51,55,59]. The main decomposition mechanism is chain scission with volatile products of phenol, benzene, and dibenzofuran [52,53]. Prolonged times at a high temperature could also lead to crosslinking and branching of polymer chains, which retard crystallization [52,57,60] and increase the polymer viscosity [49]. Thermal degradation not only degrades mechanical properties but also adversely affects consolidation. Thus, the processing time should be adjusted depending on the temperature. Table 1 gives the maximum process times recommended for different temperatures.

In previous studies [9,14], an upper limit was simply imposed on process temperature to avoid degradation. However, not only the temperature level reached but also the time spent at that temperature is important in determining the degree of degradation in the polymer. James and Black [18] used isothermal thermal degradation data to determine the upper temperature limit corresponding to a time span, which was then used to develop a process window for filament winding. However, they did not calculate the degradation weight loss in the process, so their approach was not reliable. Also, degradation data for polymers are usu-

Table 1. Suggested maximum process time at various processing temperatures for APC-2 in an oxygen-free environment [48].

Temperature	Suggested Maximum Times
400°C	2 hours
450°C	15 minutes
500°C	2 minutes
550°C	15 seconds
600°C	2 seconds

ally not available for the very high temperatures common to the tape-placement process. Therefore, a degradation kinetics model should be included in the process model to realistically determine the upper limit on heat input.

The crystallinity of the matrix affects the mechanical performance of the composite [61–79]. As a first step to control part quality, therefore, one should be able to estimate the change in morphology during the process and determine the effects of processing parameters on the crystallization behavior of the matrix. It would then be possible to tailor the processing parameters to obtain optimum properties.

Crystallization rates are usually measured under isothermal conditions using differential scanning calorimetry (DSC). It is also possible to measure crystallization rates under nonisothermal conditions using DSC. However, due to limitations imposed by the equipment, only a narrow range of cooling rates, which are much lower than found in common manufacturing processes, is possible. Hence, mathematical models that are based on theory yet practicable are required to extrapolate isothermal and nonisothermal data and to predict crystallization behavior during processing.

Most of the crystallization models used in the literature are based on theoretical work by Avrami [80–82], Tobin [83–85] and Malkin [86,87]. Although they were originally intended for isothermal crystallization, these models have been modified to describe nonisothermal crytallization [1,5,88–102].

Application of crystallization models has usually been restricted to matched die molding [1–3,90], where temperature control is relatively easier. In the tape-placement process, however, the temperature history the material experiences is much more complex. The area exposed to the heat source is remelted, and some or all of the initial crystallinity is destroyed. In subsequent lay-ups, the degree of crystallinity may increase through annealing in regions subject to high temperatures. When the polymer is raised to a temperature above its melting temperature but not high enough to melt the last traces of the crystalline phase, the surviving crystals will serve as nucleation sites on subsequent cooling [103–106]. Consequently, crystallization and nucleation rates are enhanced. On the other hand, too high a temperature reduces the number of residual nuclei and therefore retards crystallization. During the tape-placement process, different parts of the laminate experience different temperatures in the melt. As a result, a more general for-

mulation of crystallization is needed to accurately describe the complex phenomena of remelting, resolidification, and annealing.

Mantell and Springer [13] used the model proposed by Lee and Springer [1] to predict crystallinity levels in the tape-placement process. Nejhad et al. [107] applied the model developed by Velisaris and Seferis [88] to the filament-winding process. The former model is based on the Ozawa equation and the latter on the Avrami equation. None of the models includes the effect of melt temperature on crystallization. Besides, model constants depend on the cooling rate. Therefore, they cannot be used reliably at high cooling rates, for which experimental data are not available. In the current study, the model proposed by Choe and Lee [94] is chosen for process modeling of crystallization. It includes the effect of melt temperature and correlates well with nonisothermal crystallization data. The kinetic parameters are also independent of the cooling rate.

In the tape-placement process, during the placement of a layer, previous layers also experience high temperatures, and the crystallinity at those layers continues to increase. Although neglected in the previous studies, this effect is quite important in determining the finite crystallinity level of the material. In the present study, therefore, the entire lay-up process is considered for crystallinity calculations.

The crystallization model is coupled with a heat transfer model. The heat transfer model is applicable to different types of heat sources. The mold is included in the analyzed control volume. The control volume also contains the boundary between the tape and the substrate. Temperature-dependent material properties and heat generation due to crystallization are also taken into account. Temperature-dependent properties include density, thermal conductivity and heat capacity. These effects, usually neglected in the previous studies, are included to correctly calculate the thermal degradation weight loss, which is very sensitive to temperature, especially when it is high.

2. FORMULATION OF THE PROBLEM

Figure 2 displays the control volume, the boundaries and the coordinate system used. The y axis passes from the nip point, not the center of the roller. The mold is also included in the control volume. The figure shows the mostly likely position of the incoming tape. However, the tape is taken to be horizontal in the analysis for the purpose of simplification. wq indicates the length of the heated area. In the model, the length of the heated area is allowed to differ from the length on the tape.

2.1. Assumptions

In order to simplify the analysis, clearly identify processing parameters, and determine their effects, the most basic lay-up geometry is chosen. The plate is assumed to be a flat unidirectional laminate and made of the same material. Since thermal conductivity coefficients are components of a tensor, the model could be adapted to three-dimensional processes, where fibers run in different directions in different layers.

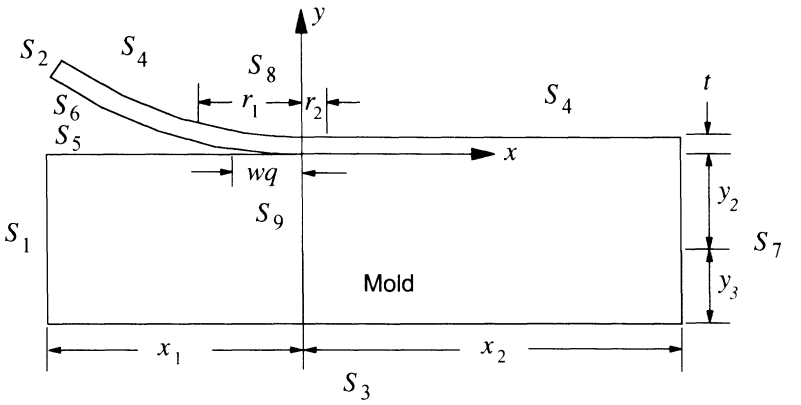

Figure 2. *The part geometry and the control volume.*

In comparison to the amount of heat supplied to melt the material, mechanical heating through deformation is assumed to be negligible. Thus, thermal and mechanical analyses are carried out separately.

Even though the composite is heterogeneous, with the fiber and matrix having different thermophysical properties, in the analysis it is treated as an anisotropic yet homogeneous continuum.

The material is uniformly heated through the width, and heat losses through the edges are negligible, so the heat conduction problem can be reduced to a two-dimensional analysis. It should be noted that uniform heating through the width is essential for uniform consolidation. Uneven heating could cause degradation at the center or incomplete consolidation at the edges [38,43]. The area exposed to the heat source is also uniformly heated through its length (wq in Figure 2). In reality, the heated area could have different absorption rates depending on how they are exposed to the heat source. For example, in the case of a laser beam, the absorption rate could change with the angle of incidence, and multiple reflections could occur [41].

A quasi-steady state is assumed to prevail throughout the process. Previous studies [9,12] showed that, because of local heating, even a very small control volume could be used for analysis to give sufficiently accurate results. Nevertheless, dimensions of this control volume will be chosen so as to render the quasi-steady state assumption valid.

If sufficient time elapses before a new layer is laid, as is the case with large structures, the incoming laminate and mold can be taken to be at the ambient temperature. The control volume is taken to be so long that the dominant heat transfer mode at the right edge is heat transport due to plate motion rather than heat conduction.

Considering that the roller is made of a highly conductive material such as steel (45 W/m°C) connected to a large structure and that the transverse heat conductivity of the laminate is very low ($\approx$0.52 W/m°C), the temperature of the

roller can be assumed to be constant. Heat flux from the laminate to the roller can then be approximated by introducing an effective heat transfer coefficient, h_r ($Wm^{-2}°C^{-1}$). In this case, the boundary between the laminate and the roller is treated as a convection boundary condition. Cogwell [48] provided effective heat transfer coefficients corresponding to various contacting media.

2.2. Boundary Conditions

For the boundary S_1 in Figure 2, the temperature is constant and equal to the laminate temperature far from the heated region

$$T = T_c \quad \text{on} \quad S_1 \tag{1}$$

For S_2, the incoming tape temperature is uniform and equal to the ambient temperature. If the tape is preheated, it is equal to the preheat temperature:

$$T = T_t \quad \text{on} \quad S_2 \tag{2}$$

Since the roller is considered as a heat sink, we have the following convection boundary condition across the contact area:

$$k_T \frac{\partial T}{\partial y} = -h_r(T - T_r) \quad \text{on} \quad S_8 \tag{3}$$

where k_T is the transverse conductivity of the laminate and T_r is the roller temperature. For the areas exposed to air, we have

$$k_T \frac{\partial T}{\partial y} = -h_a(T - T_a) \quad \text{on} \quad S_3, S_4, S_5 \text{ and } S_6 \tag{4}$$

On the right-hand side of the control volume, the temperature gradient is taken to be zero:

$$\frac{\partial T}{\partial x} = 0 \quad \text{on} \quad S_7 \tag{5}$$

The boundary conditions at the heated surfaces depend on the type of heat

Table 2. Surface heat transfer coefficients for APC-2 [48].

Contacting Surface	Surface Heat Transfer Coefficient
Water	2000 W/m²°C
Metal	400 W/m²°C
Air at 100 m/s	50 W/m²°C
Still air	10 W/m²°C

source used. If laser or IR heating is used, a heat flux boundary condition is prescribed:

$$k_T \frac{\partial T}{\partial y} = -q \quad \text{on} \quad S_9 \tag{6}$$

On the other hand, if a hot gas torch is used, the following convection boundary condition is prescribed:

$$k_T \frac{\partial T}{\partial y} = -h_{hg}(T - T_{hg}) \quad \text{on} \quad S_9 \tag{7}$$

where T_{hg} is the gas temperature.

2.3. Governing Equation

When coordinates moving with the roller are used, the governing equation for energy balance becomes [108]

$$k_L \frac{\partial^2 T}{\partial x^2} + k_T \frac{\partial^2 T}{\partial y^2} + \varrho r = \varrho C_p v_x \frac{\partial T}{\partial x} \tag{8}$$

where k_L and k_T are the longitudinal and transverse conductivities (W/m°C), respectively, of the composite, v_x is the velocity of the roller (m/s), ϱ is the density of the composite (kg/m^3), and C_p is the specific heat (J/kg°C). The heat source r (J/kg sec) accounts for the heat release from crystallization

$$r = m_m \frac{dH}{dt} \tag{9}$$

where H is the heat of melting of the semi-crystalline thermoplastic matrix at time t, and m_m is the mass fraction of the matrix. H is related to the mass fraction crystallinity by

$$c_m = \frac{H}{H_f} \tag{10}$$

Here H_f is the heat of melting of a fully crystalline phase. The rate of heat generation is thus expressed as

$$r = m_m H_f \frac{dc_m}{dt} \tag{11}$$

Due to the steady-state nature of the process, the temperature and crystallinity

fields within the control volume do not change with time. Thus, Equation (11) becomes

$$r = m_m H_f \frac{\partial c_m}{\partial x} v_x \tag{12}$$

Substituting Equation (12) into Equation (8), we finally obtain

$$k_L \frac{\partial^2 T}{\partial x^2} + k_T \frac{\partial^2 T}{\partial y^2} + \varrho m_m H_f v_x \frac{\partial c_m}{\partial x} = \varrho C_p v_x \frac{\partial T}{\partial x} \tag{13}$$

Crystallinity levels within the laminate are calculated using the crystallization kinetics model. Since crystallization is a strong function of temperature, thermal and crystallization analyses are fully coupled.

2.4. Crystallization Kinetics

The model developed by Choe and Lee [94] for nonisothermal crystallization of PEEK is adopted to describe crystallization kinetics during the tape-placement process. Although the model was developed for neat resin, it is assumed to be applicable to carbon-fiber-reinforced PEEK. This assumption is based on the experimental data [1,70,88,95], which show that crystallization rates for APC-2 and neat PEEK resin are comparable. The model is based on the Tobin equation for isothermal phase transformation kinetics [83–85]:

$$\frac{\alpha(t)}{1 - \alpha(t)} = N_o k G^n t^n + I^* k G^n \int_0^t (t - \tau)^n [1 - \alpha(\tau)] d\tau \tag{14}$$

Here, τ is a dummy integration constant, and α is the volumetric relative crystallinity defined as

$$\alpha = \frac{c_v(t)}{c_v(\infty)} \tag{15}$$

where c_v is the volume fraction crystallinity at time t, and $c_v(\infty)$ is the volume fraction crystallinity at infinite time for the given temperature. N_o is the number of heterogeneous nuclei per unit volume, which decreases with increasing melt temperature as shown in Figure 3, G is the growth rate of spherulites, I^* is the number of homogeneous nuclei formed per unit untransformed volume per second, the exponent n is 3, and k is $4\pi/3$ for three-dimensional growth of spherulites. The first part of Equation (14) accounts for the effect of heterogeneous nucleation, and the second one the effect of homogeneous nucleation. In heterogeneous nucleation, a number of growth nuclei exist at the beginning of the transformation and start to grow instantaneously. On the other hand, in homoge-

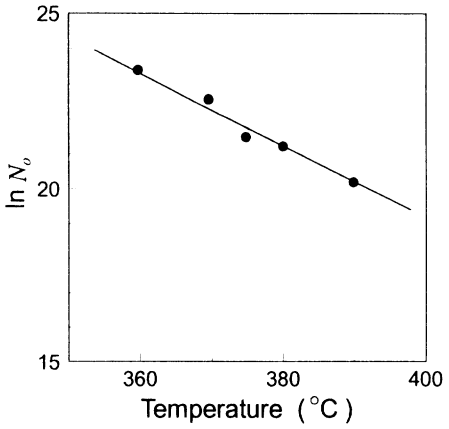

Figure 3. *Plot of the number of heterogeneous nuclei per unit volume,* N_0*# of nuclei/cm*^{3}*), as a function of melt temperature [94].*

neous nucleation, nuclei of the new phase start to appear at random and grow in the untransformed material throughout the process.

Mass fraction crystallinity can be obtained from the volumetric crystallinity by the following formula:

$$c_m = \frac{c_v \varrho_c}{c_v \varrho_c + (1 - c_v)\varrho_a} \tag{16}$$

where ϱ_c is the density of the crystalline phase, and ϱ_a is the density of the amorphous phase.

Equation (14) could describe only isothermal crystallization. Nonisothermal crystallization analysis requires crystallization rates to be calculated. Assuming that isothermal crystallization rates can be superposed to obtain nonisothermal crystallization rates, we first differentiate Equation (14) to obtain [94]

$$\dot{\alpha}(t) = N_o k n G^n t^{n-1}[1 - \alpha(t)]^2 + I^* k n G^n [1 + \alpha(t)]^2 \int_0^t (t - \tau)^{n-1}[1 - \alpha(\tau)]d\tau \tag{17}$$

Choe and Lee [94] used the following values of G [109] and I^* [110]:

$$G = G_o \exp\left(-\frac{E_d}{RT}\right) \exp\left(-\frac{\Psi_1 T_m^o}{T(T_m^o - T)}\right) \tag{18}$$

$$I^* = I_o \exp\left(-\frac{E_d}{RT}\right) \exp\left(-\frac{\Psi_2 T_m^o}{T(T_m^o - T)}\right) \tag{19}$$

where T_m^o is the equilibrium melting temperature, E_d is the activation energy of diffusion of crystallization segments across the phase boundary, Ψ_1 is related to the free energy of formation of a critical nucleus, Ψ_2 is a constant related to the free energy of formation of a growth embryo, and G_o is a universal constant for semi-crystalline polymers.

Substituting these values for I^* and G into Equation (17) yields the following equation for the true ratio of change of the volumetric crystallinity:

$$\frac{\dot{c}_v(t)}{c_v(\partial)} = k_1 \exp\left(-\frac{3E_d}{RT}\right) \exp\left(-\frac{3\Psi_1 T_m^o}{T(T_m^o - T)}\right) t^2 \left[1 - \frac{c_v(t)}{c_v(\infty)}\right]^2$$
$$+ k_2 \exp\left(-\frac{4E_d}{RT}\right) \exp\left(-\frac{(3\Psi_1 + \Psi_2)T_m^o}{T(T_m^o - T)}\right) \left[1 - \frac{c_v(t)}{c_v(\infty)}\right]^2$$
$$\times \int_0^\tau (t - \tau)^2 \left[1 - \frac{c_v(\tau)}{c_v(\infty)}\right] d\tau \tag{20}$$

where k_1 and k_2 are given by

$$k_1 = 4\pi N_o G_o^3$$
$$k_2 = 4\pi I_o G_3 \tag{21}$$

Choe and Lee [94] determined the constants in Equation (20) by a nonlinear regression analysis of nonisothermal data. Crystallization as described by Equation (20) occurs only when the temperature is between the melting temperature (T_m) and the glass transition temperature. That is, time t in Equation (20) elapses only in this temperature range.

Since Equation (2) could explain only the crystallization behavior of a polymer, the model developed by Maffezzoli et al. [6,7] is used to describe the crystal melting kinetics of the process. Melting of the crystallites for PEEK is described by

$$c_v(t) = c_v(t_{in})\left(1 - 0.5 \int_{t_{in}}^{t} K dt\right)^2 \tag{22}$$

where t_{in} is the initial time. K is described by an Arrhenius relation:

$$K = K_o \exp\left(-\frac{E_a}{RT}\right) \tag{23}$$

Equation (20) is used during cooling from the melting temperature (T_m) to the glass transition temperature and during heating from glass transition up to 320°C. Equation (22) is used during heating from 320°C and whenever the temperature is above the melting temperature (345°C). Below glass transition, the crystallization rate is assumed to be zero. During heating, the transition temperature between crystallization and melting is chosen to be 320°C, where both models predict very small rates. The initial crystallinity and time, $c_v(t_{in})$ and t_{in} in Equation (22), are then the values resulting from Equation (20) at 320°C during heating. Figure 4 shows the handling of the time, t, in the crystallization model. The time, t, in Equation (20) starts from the zero value as soon as the glass transition point (145°C) is reached. With regard to melting, two conditions, can be considered. The crystallites could be completely melted. In this case, the time, t, starts from the zero value at 345°C (T_m) during cooling as shown in Figure 4(a). On the other hand, if the crystallites are partially melted, the time

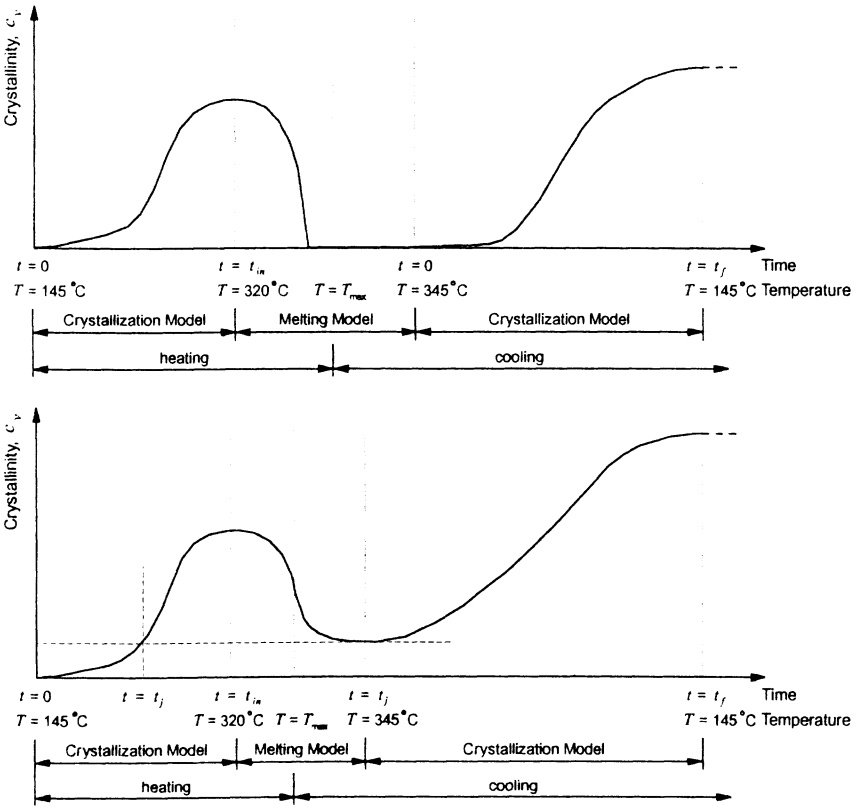

Figure 4. *Handling of the time in the crystallization model: (1) complete melting (b) partial melting.*

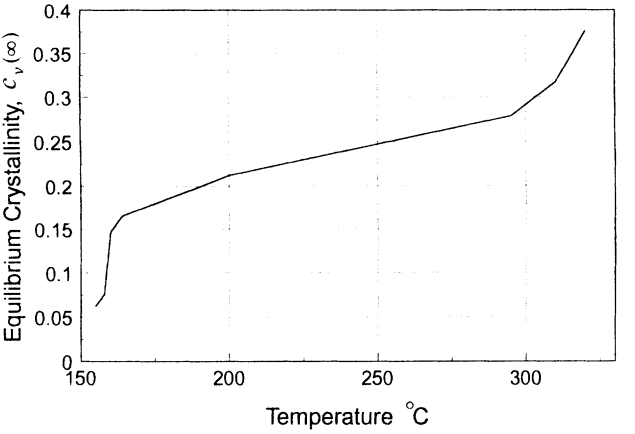

Figure 5. *Isothermal crystallization data for PEEK [88,93,104,111,112].*

t assumes the value corresponding to the crystallinity during crystallization that has the same value as the crystallinity attained at the end of the melting [Figure 4(b)].

Equation (20) requires a value for the equilibrium crystallinity $c_v(\infty)$. The available data indicates the equilibrium crystallinity falling off with decreasing temperature (Figure 5). Therefore, in this study, unlike the model developed by Choe and Lee [94], the equilibrium crystallinity is assumed to be temperature dependent and is obtained from Figure 5 by interpolation. When the crystallinity at a temperature exceeds the corresponding equilibrium crystallinity level—i.e., when the relative crystallinity α is greater than unity—the resulting crystallization rate is assumed to be zero. Accordingly, time t in Equation (20) does not elapse.

2.5. Degradation Kinetics

The degradation kinetics model developed by Nam and Seferis [58] is adopted to estimate the degradation weight loss in the tape-placement process. The model is applicable to PEEK in a nitrogen atmosphere. Degradation of PEEK in air is severer and more complex than in nitrogen [55,56]. However, the controlling mechanism of degradation in air is transport of oxygen through the melt. Since under fast heating conditions, oxygen diffusion is very slow in comparison to the temperature change, additional degradation due to oxidation can be neglected [55]. In tape placement, where heat-up and cool-down rates are well above 3000°C/min, dwell times at high temperatures are very short. Therefore, the same degradation kinetics model as developed in a nitrogen atmosphere will be applied to the tape-displacement process regardless of the type of heat source being used.

The amount of degradation α_d is given by the ratio of the current weight loss to the final weight loss:

$$\alpha_d = \frac{M_o - M}{M_o - M_f} \tag{24}$$

where M, M_o and M_f are the current, initial and final weights of the polymer, respectively.

The degradation rate is assumed to be the sum of the contributions of two competing mechanisms [58] for PEEK:

$$\frac{d\alpha_d}{dt} = k[w_1(1 - \alpha_d) + w_2\alpha_d(1 - \alpha_d)] \tag{25}$$

where w_1 and w_2 are weight factors and k is a rate constant described by an Arrhenius relation:

$$k(T) = A \exp\left(-\frac{E}{RT}\right) \tag{26}$$

The final weight is taken to be 0.64 M_o [58]. Reduction in the weight of the polymer is then expressed as

$$\text{Weight Loss } (\%) = 36\alpha_d \tag{27}$$

2.6 Solution of the Problem

Finite element formulation of the problem is given in Appendix A. Figure 6 shows the mesh structure, in which nonuniform rectangular elements are used. The final Equation (A.22) is given by

$$\{T_u\} = [K_{uu}]^{-1}(\{P_u\} - [K_{us}]\{T_s\}) \tag{28}$$

Given the boundary conditions, material properties, and heat generation, unknown node temperatures can be calculated from Equation (28). However, density ϱ, thermal conductivities k_L and k_T, and specific heat C_p are functions of temperature. Consequently, $[K_{uu}]$, $[K_{us}]$, and $\{P_u\}$ will contain temperature-dependent terms. Besides, the effect of heat generation through crystallization is also included in the heat transfer analysis. Calculation of the crystallization rates will then require the temperature field within the laminate, which is not known at the beginning. In order to tackle this problem, an iterative solution procedure was followed. In the first iteration, average values of the temperature-dependent material properties were used and crystallization rates were not calculated. In subsequent iterations, nodal temperatures obtained in the previous iteration were used to determine temperature-dependent material properties and crystallization rates.

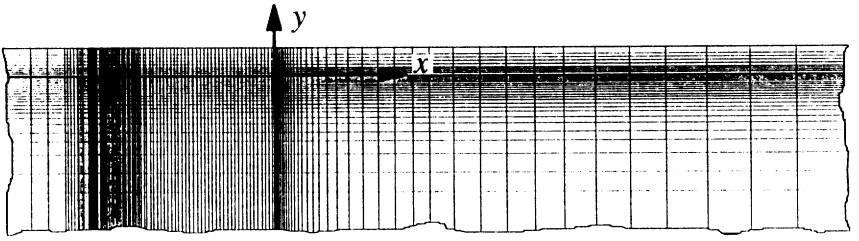

Figure 6. *Part of the mesh structure used in the analysis. Horizontal and vertical dimensions are not on scale.*

In order to determine crystallization rates, temperature profiles at the center and top of each ply were calculated from the nodal temperatures by linear interpolation. Material entering the control volume experiences this temperature field within the time set by the roller velocity. Given the temperature history, crystallinity levels within each ply were calculated using Equations (20) and (22). From this data, crystallinity gradients (dc_m/dx) at the center of each element were then found by interpolation and incorporated into the heat transfer analysis by Equation (A.19).

The iterative process is continued until the maximum difference in temperature profiles obtained in two consecutive iterations becomes less than 1°C. After five or eight iterations, the maximum difference usually satisfies this requirement.

In every lay-up, crystallinity levels in previously laid plies are updated unless the maximum temperature in a certain ply is below the glass transition temperature or the crystallinity is higher than the equilibrium crystallinity for that temperature.

Since the interface between the freshly laid layer and the substrate experiences the highest temperature, it is subject to the severest thermal degradation, which leads to poor mechanical properties. Excessive degradation at the interface also adversely affects bonding. In this respect, layer interfaces are the most critical portions of the laminate. Degradation weight loss is then calculated at the interface between the fresh tape and the substrate using the temperature field obtained in the last iteration. The calculations are performed for temperatures above 400°C. In subsequent lay-ups, if the same interface is again subjected to critical temperatures, weight loss calculation is extended to those lay-ups.

3. RESULTS

A computer code was developed for the aforementioned solution procedure. Temperature profiles and crystallinity levels within the laminate were obtained for different sets of process parameters.

3.1. Verification

The model is verified by comparing the results with an available analytical

solution [12] developed for a simpler case. The analytical model has its limitations, as mentioned in reference [12]. Therefore, it cannot be used for a parametric study of the tape-placement process. Comparison is made for a steady-state heat transport problem similar to the tape-placement process, except that there is no boundary between the tape and the substrate, and the area exposed to the heat source is the top surface. The laminate in this case consists of 40 plies. The material is transversely isotropic. Analytical and numerical results are compared for two different roller velocities, 50 and 200 mm/s. Input parameters are given in Reference [12]. As shown in Figure 7, analytical and numerical results agree well. Maximum discrepancy occurs at the top surface. Even at one ply below the surface, however, the difference between the two temperature profiles is insignificantly small. Also, the results of the present numerical model agree well with the experimental data reported by Mantell et al. [24].

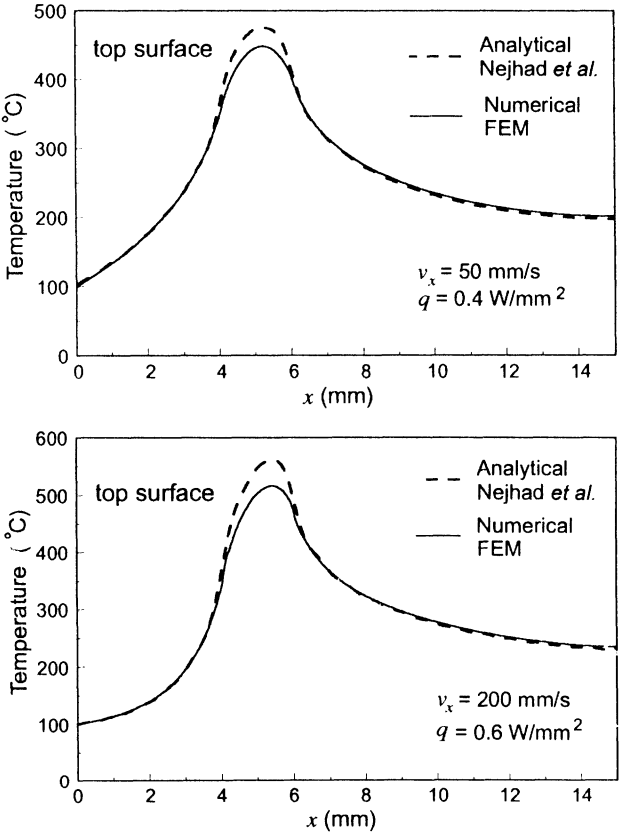

Figure 7. *Comparison between the analytical and the numerical solutions at the top surface of the laminate for* v_x = *50 mm/s and* v_x = *200 mm/s.*

Table 3. Material property data for APC-2.

ϱ, density (temperature dependent)	ref. 3
First iteration value	1560 kg/m^3
ϱ_c, density of fully crystalline PEEK [104]	1.4006 g/cm^3
ϱ_a, density of amorphous PEEK [104]	1.2626 g/cm$_3$
Initial tape crystallinity [112]	0.0
T_m, melting temperature [73,74]	345°C
T_g, glass transition temperature [104]	145°C
k_L, longitudinal conductivity (temperature dependent)	ref.48
First iteration value	6.0 W/m°C
k_T, transverse conductivity (temperature dependent)	ref. 48
First iteration value	0.72 W/m°C
C_p, heat capacity (temperature dependent)	ref. 48
First iteration value	1425 J/kg°C
H_f, heat of melting of fully crystalline phase [104]	130 kJ/kg
m_m, mass fraction of the matrix [48]	0.32
E_d, activation energy for diffusion, Equation (20) [94]	1.52×10^4 (cal/mol)
k_2, kinetic constant, Equation (20) [94]	9.32×10^{38} sec^{-4}
Ψ_1, kinetic constant, Equation (20) [94]	802°C
Ψ_2, kinetic constant, Equation (20) [94]	1790°C
G_o, universal constant for polymers, Equation (21) [94]	75,000 cm/sec
T_m^o, equilibrium melting temperature [94,113]	385°C
n, exponent for crystallization [94]	3
K_o, kinetic constant for melting, Equation (23) [7]	exp(73) sec^{-1}
E_a, activation energy for melting, Equation (23) [7]	397 kJ/mol
A, preexponential factor, Equation (26) [58]	8.265×10^{12} sec^{-1}
E, activation energy, Equation (26) [58]	240.2 kJ/mol
w_1, weight factor, Equation (25) [58]	0.0215
w_2, weight factor, Equation (25) [58]	0.9785

3.2. Inputs for the FEM Code

Properties for the materials used in the program—carbon-fiber-reinforced polytheretherketone, APC-2—are given in Table 3. The mold is made of steel and its material property data are given in Table 4. Table 5 gives the input parameters regarding specimen geometry (Figure 2), processing variables, boundary conditions and mesh configuration.

In order to determine the upper bound for the heat input, the degree of matrix degradation caused by high process temperatures should be determined. Maxi-

Table 4. Material property data for the steel mold [4].

k_b, conductivity	45 W/m°C
C_b, heat capacity	473 J/kg°C
ϱ_b, density	7800 kg/m^3

Table 5. Input parameters for the FEM code.

Geometry of the Specimen and the Base Frame	
Thickness of the tape, t [48]	0.125 mm
Number of plies in the substrate	20
Thickness of the base frame, y_3	10 mm
Experimental Variables and Boundary Conditions	
Roller velocity, v_x	50 mm/s
Heated length on the tape or the substrate, wq	4 mm (laser), 15 mm (Hot gas)
Heat flux (laser), q	2.1 W/mm^2
Temperature of the hot gas, T_{hg}	795°C
Heat transfer coefficient of the hot gas, h_{hg}	2500 W/m^2°C
Ambient temperature, T_a	25°C
Heat transfer coefficient of air, h_a	10 W/m^2°C
Contact length in negative x direction, r_1	10 mm
Contact length in positive x direction, r_2	3 mm
Temperature of incoming substrate and mold, T_c	25°C
Temperature of incoming tape, T_t	25°C
Roller temperature, T_r	25°C
Heat transfer coefficient of the roller, h_r	400 W/m^2°C
Control Volume Size and Mesh Configuration	
Analyzed length in negative x direction, x_1	15 mm (laser), 25 mm (Hot gas)
Analyzed length in positive x direction, x_2	80 mm (laser), 100 mm (Hot gas)
Number of elements	5600
Number of horizontal divisions	170
Number of vertical divisions	35

mum temperature control is not adequate as a degradation criterion for the tape-placement process. The material is more likely to undergo severe degradation at slow roller speeds due to more time spent at high temperatures. Using a degradation kinetics model to determine the weight loss during the process is therefore a more reliable approach. From the data given in Table 2, the maximum allowable weight loss was estimated to be 0.01%. Since bonding is achieved in shorter times at higher processing temperatures, the interface temperature should be raised as high as possible without causing excessive degradation. Therefore, in the following results, the maximum allowable weight loss (0.01%) is used as a degradation criterion to select the heat input.

3.3. The Effect of Roller Velocity

Temperature fields within a 20-ply laminate during the placement of the 21st layer are shown in Figure 8 for two roller velocities, 5 and 50 mm/s. The dashed

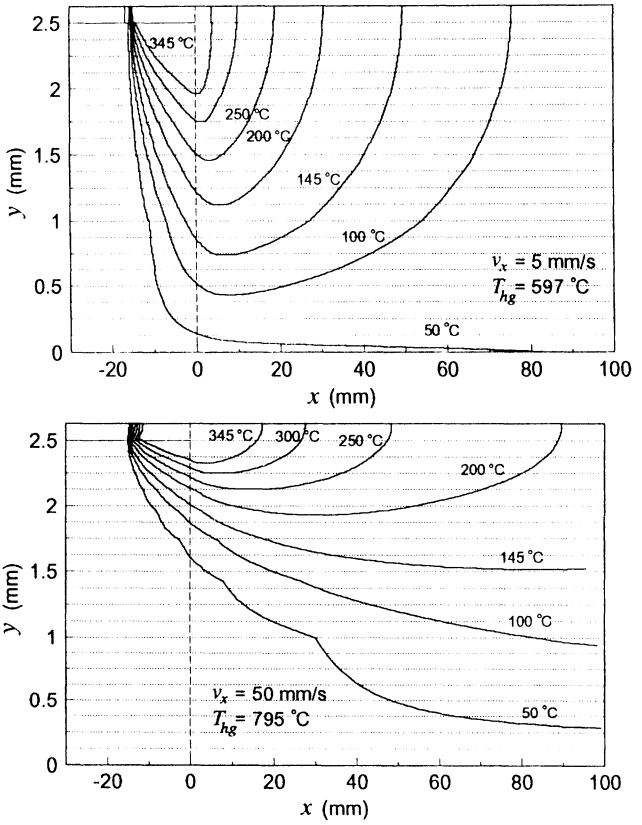

Figure 8. *Temperature fields within a 20-ply laminate during the placement of the 21st layer for two different roller speeds. Hot gas heating is used.*

lines show the layer interfaces. The vertical line shows the y axis, which passes through the nip point. At low speeds, heat transfer is dominated by conducting rather than heat transport. Temperature inside the laminate substantially increases due to heat conduction from the interface. At very high speeds, heat transfer is dominated by heat transport. Only regions close to the heated surface are raised to high temperatures. Roller velocity thus significantly affects bonding behavior. Bonding starts at the nip point, where the tape and the substrate merge ($x = 0.0$), and continues as long as the interface is subject to high tempertures. Bonding occurs mostly above the melting temperature (345°C). Considering that, in the figure, temperature fields are presented in terms of position, the time spent in melt is longer at low speeds. Also, previous interfaces melt and bonding continues at those interfaces. As shown in Figure 8(a), the melt zone is large for the low speed. Four layers below the tape are melted. On the other hand, for the high speed, only one layer is melted. For high roller speeds, bonding time may then become too short to achieve full consolidation. However, at low roller speeds, as the time spent in the melt increases, thermal degradation becomes severer. Heat input, and thus temperature at the interface, should then be reduced for low speeds to avoid violating the degradation constraint. For a roller speed of 5 mm/s [Figure 8(a)], the maximum temperature at the interface is 480°C; for 50 mm/s [Figure 8(b)], it is 565°C. Since bonding is a temperature-driven process, high temperatures are more conducive to bonding. We may conclude that there exists an optimum velocity that will offer a compromise between these conflicting effects.

In comparison to hot gas heating (Figure 8), laser heating (Figure 9) results in smaller melt zones and shorter bonding times. The main reason seems to be the small heated length used for the laser heating. The laser beam is too concentrated to heat a substantial part of the laminate.

Figure 10 shows the relationship between the roller speed and the heat input for both laser and hot gas heating. The heat input increases at the same rate as the velocity.

3.4. The Effect of Preheating

Preheating the substrate greatly affects the resulting temperature field as shown in Figure 11. The substrate was preheated to 150°C together with the mold while the tape was kept at room temperature. Ths most striking consequence of preheating is the significant increase in residence time in the melt due to the slower cooling rate. Comparing Figure 11 to Figure 8, the melt zone is quite extensive for the preheated substrate.

Preheating both the tape and the substrate or preheating the roller does not improve bonding conditions. The tape already experiences unnecessarily high temperatures. Preheating the tape or the roller only causes more degradation.

3.5. The Effect of Heated Length

Changing the heated length (wq in Figure 2) greatly affects the temperature field as shown in Figures 12 and 13. The effect of larger heated lengths [Figure 12(b) and 13(b)] is similar to the effect of preheating the substrate in slowing

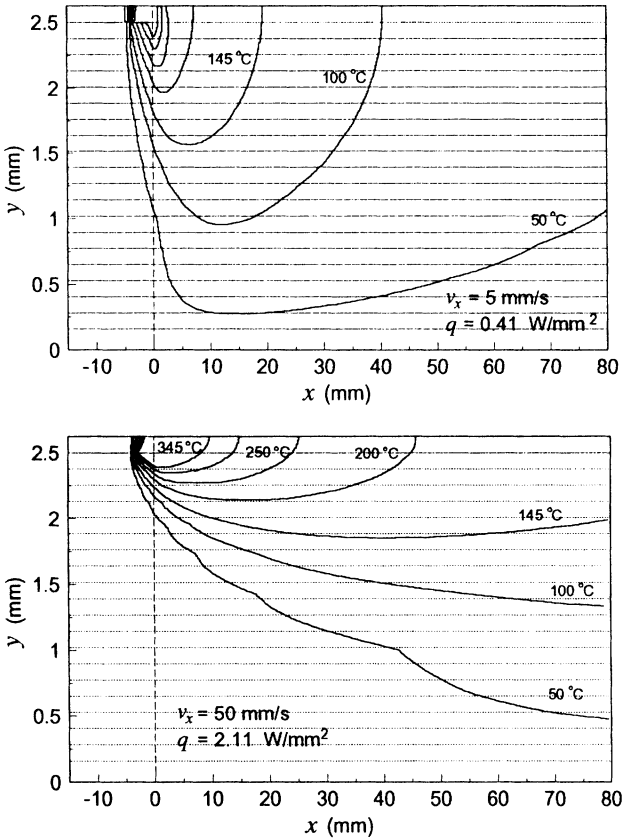

Figure 9. *Temperature fields within a 20-ply laminate during the placement of the 21st layer for two different roller speeds. Laser heating is used.*

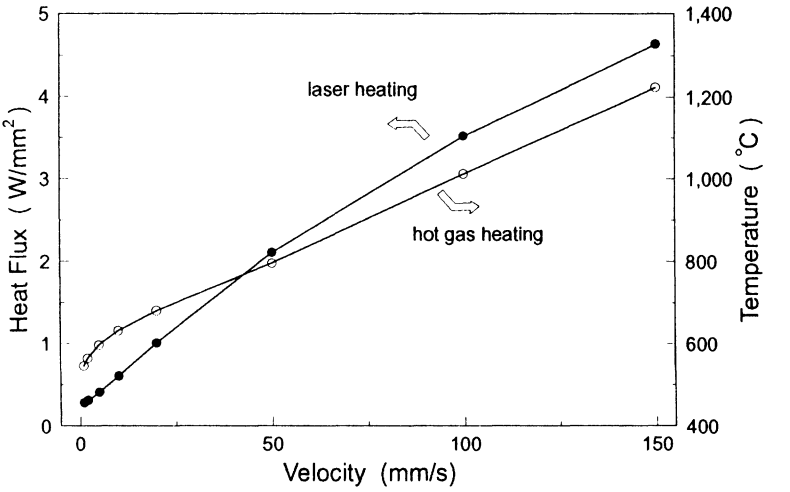

Figure 10. *The relationship between the roller speed and the heat input when the degradation criterion is used.*

down the cooling rate and thus increasing the residence time in the melt. On the other hand, small heated lengths result in very small melt zones and thus very short residence times. Using a large heated length is then more favorable to consolidation quality. Considering that bonding could start only at the nip point and a larger heated length means more degradation, choosing too large a heated length may not improve consolidation. In this case, in order to prevent degradation at the heated zone, heat input and thus the temperature should be reduced. For a heated length of 5 mm [Figure 12(a)], the maximum temperature at the interface is 506°C; for 25 mm [Figure 12(b)], it is 460°C. We may expect that there is an optimum value for the heated length that reaches a compromise among these conflicting effects.

When the tape and the substrate are heated equally, the tape usually experiences temperatures higher than the substrate. Unnecessarily high tape temperatures increase thermal degradation and cause a reduction in the maximum possible heat input. Therefore, more heat should be supplied to the substrate. Figure 14 presents the temperature fields resulting from unbalanced heating. The ratio of the heated length on the substrate to the length on the tape (η) was 2:1. The total heated length, however, was kept constant ($2wq = 30$ mm). In comparison to the case presented in Figure 8, consolidation conditions are significantly improved. The melt zone becomes very large. The ratio of the heated length is then an important parameter in optimizing the process.

3.6. The Effect of Processing Parameters on Crystallinity

Recommended levels of crystallinity for carbon-fiber-reinforced polyether-etherketone are between 25 and 35% [48], which can be achieved by a cooling

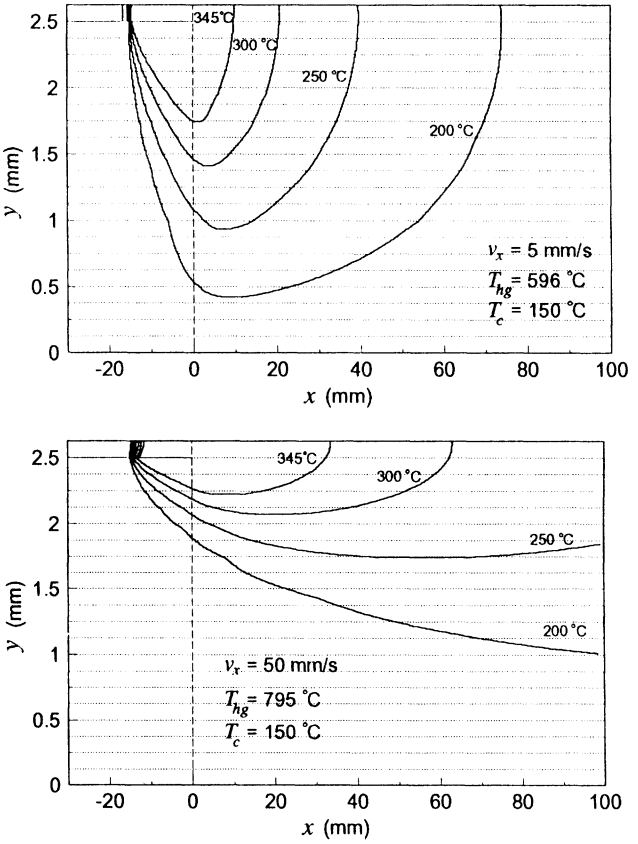

Figure 11. *Temperature profiles along the length of a 20-ply laminate preheated to 150°C for two different roller speeds.*

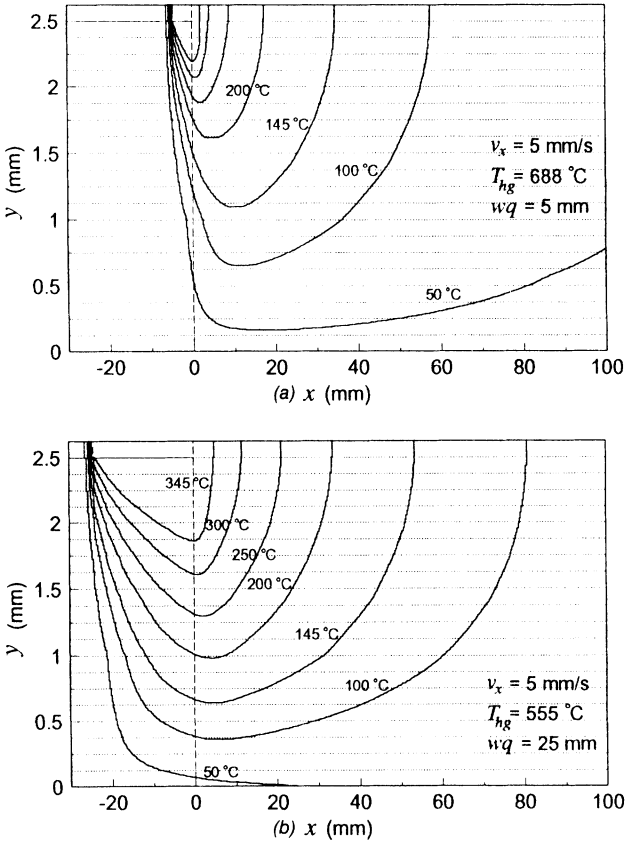

Figure 12. *Temperature fields for two different heated lengths. (a)* wq = *5 mm, (b)* wq = *25 mm.* v_x *is 5 mm/s.*

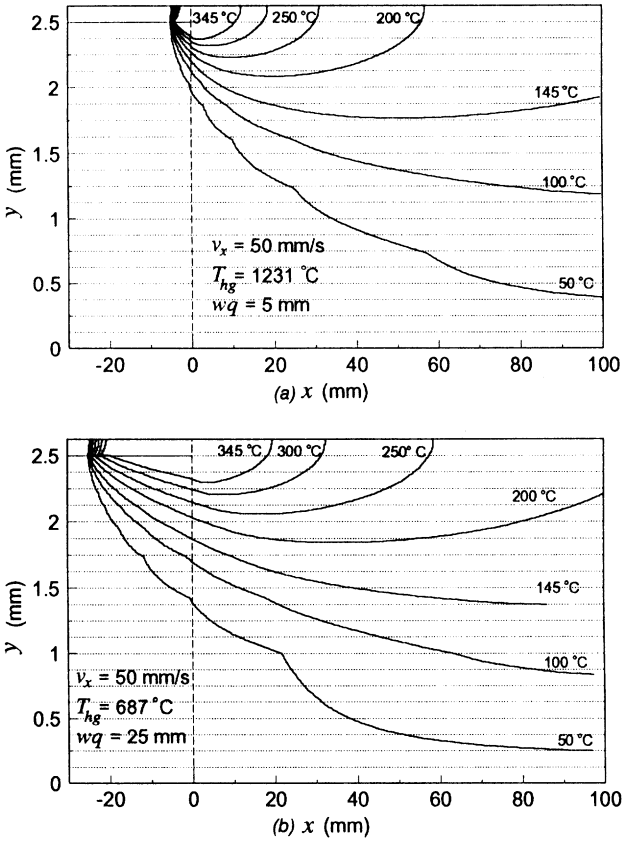

Figure 13. *Temperature fields for two different heated lengths. (a)* wq *= 5 mm, (b)* wq *= 25 mm.* v_x *is 50 mm/s.*

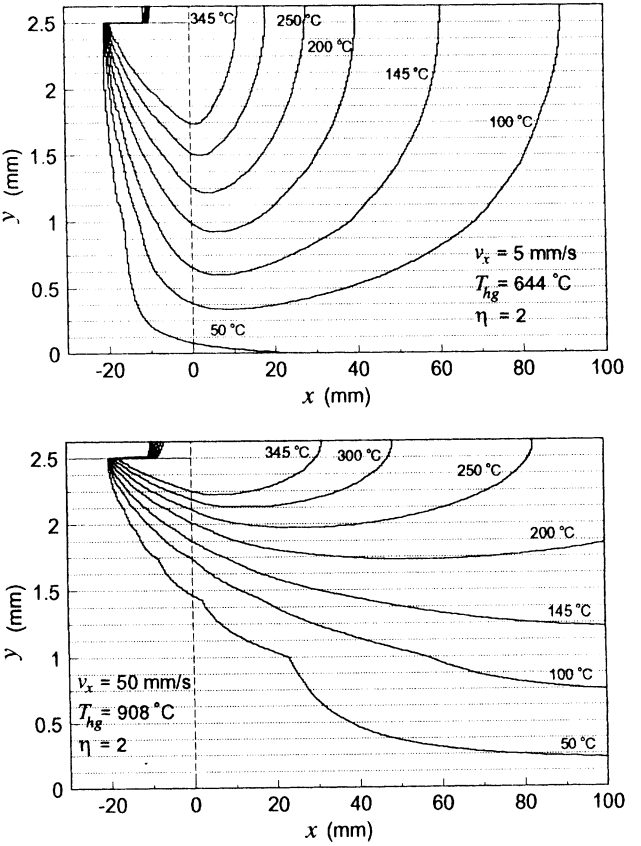

Figure 14. *Temperature fields when the ratio of the heated length on the laminate to the heated length on the tape is 2:1.*

rate between 6 and 600°C/min [48]. However, in the tape-placement process, cooling rates are very high, typically well above 3000°C/min.

Figure 15 shows the temperature profiles experienced by the top surface of the 20th ply during a 40-ply lay-up process and the corresponding crystallinity development for a 0.1 m/s roller speed. Laser heating was used for the crystallinity results. The analyzed length in the positive x direction, x_2, is increased to obtain the full temperature profile above the glass transition temperature. Since the degradation criterion yields a different heat input for each lay-up due to the effect of laminate thickness, heat input is changed for each layer. Crystallization time t is defined in section 2.4. As Figure 15(b) shows, maximum crystallinity in the ply is less than 0.006. Because of local heating, only the regions very close to the area exposed to the heat source are heated above the glass transition temperature. This will cause large temperature gradients and, thus, high cooling rates. As

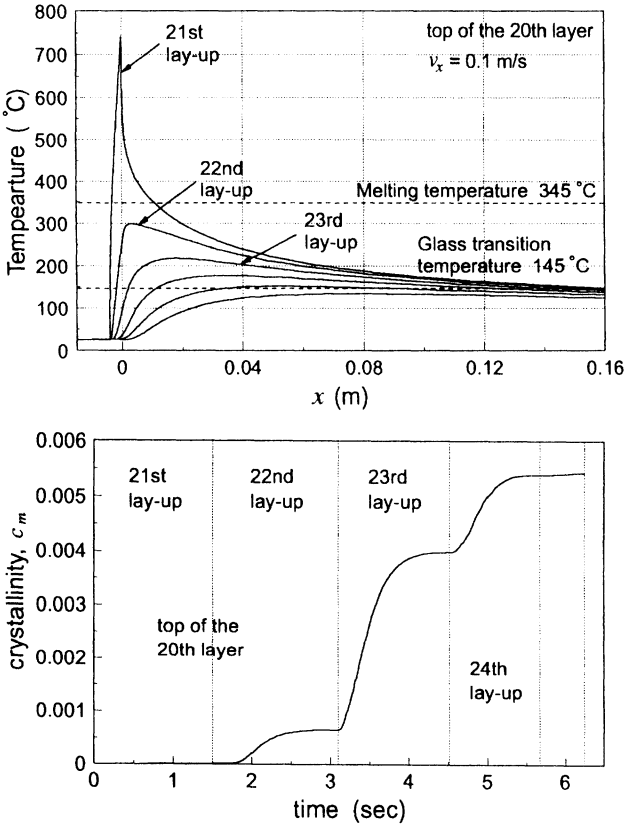

Figure 15. *Temperature profiles experienced by the top surface of the 20th ply during subsequent lay-ups and the corresponding crystallinity development for* v_x = *0.1 m/s.*

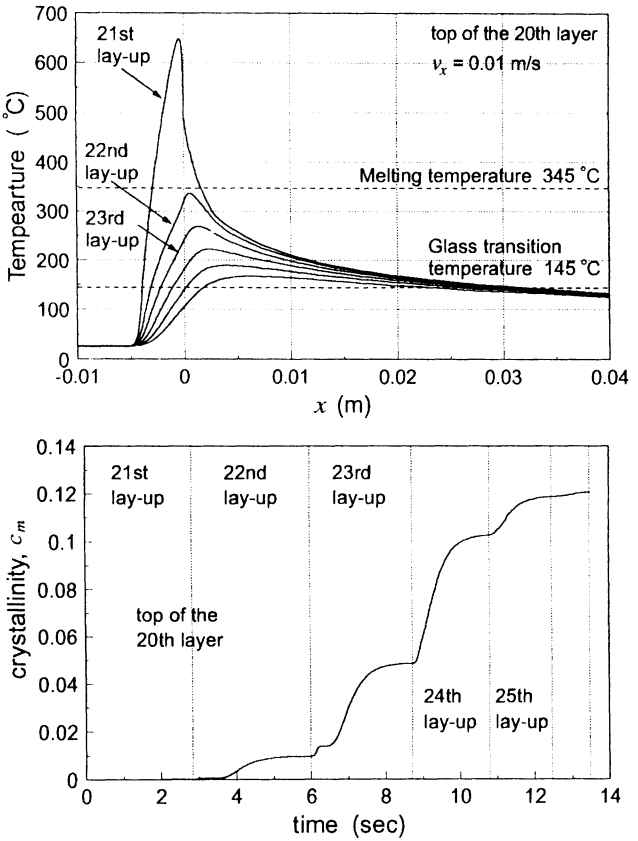

Figure 16. *Temperature profiles experienced by the top surface of the 20th ply during subsequent lay-ups and the corresponding crystallinity development for* v_x = *0.01 m/s.*

shown in the figure, after four additional lay-ups, the maximum temperature in the 20th ply falls below the glass transition temperature, and hence further crystallization is not possible. Further lay-ups no longer increase the crystallinity in the 20th ply.

Reducing the roller velocity to 0.01 m/s results in lower temperature gradients (Figure 16). During the placement of five subsequent layers, the same ply experiences temperatures above the glass transition point. Even though crystallinity increases significantly due to slower cooling rates and longer annealing times, it is still far below the recommended levels.

Preheating the substrate greatly affects crystallinity levels. Figure 17 shows the temperature profiles and the corresponding crystallinity development for 0.1 m/s roller speed when the substrate is preheated to 100°C. The crystallinity level, although still below the optimum value, is significantly increased because of slo-

wer cooling rates and longer annealing times. Figure 18 presents layerwise final crystallinity levels. Little or no crystalline material forms at the top of the laminate due to shorter annealing times. The bottom of the laminate is also amorphous due to very high cooling rates caused by excessive heat loss to the steel mold.

When the roller velocity is reduced to 0.01 m/s, crystallinity levels are increased (Figures 19 and 20). However, the top and bottom of the laminate are still amorphous.

When the preheat temperature is above the glass transition temperature, uniform crystallinity levels within the recommended range can be obtained for low roller speeds, as shown in Figure 21. Therefore, if the laminate is not preheated or is preheated to low temperatures, heat treatment is needed to raise the laminate

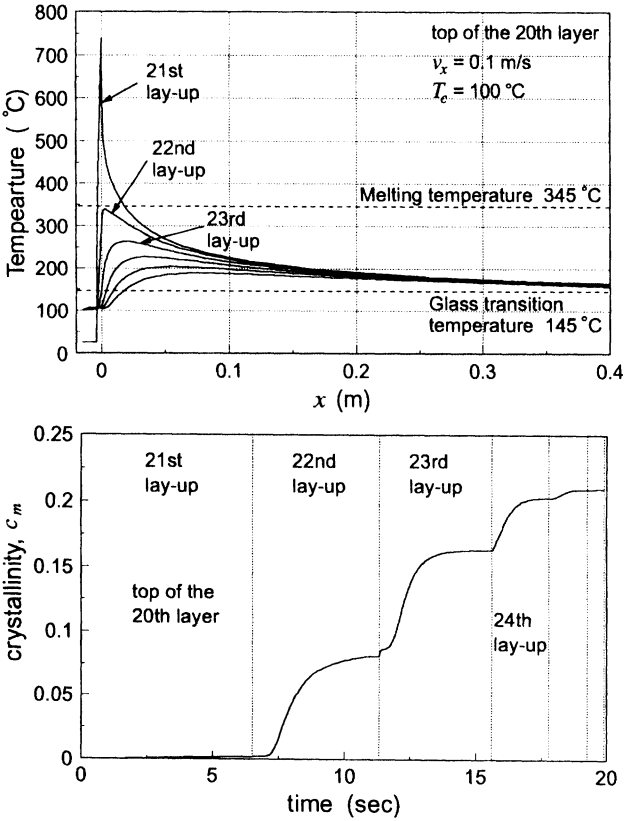

Figure 17. *Temperature profiles experienced by the top surface of the 20th ply during subsequent lay-ups and the corresponding crystallinity development for* v_x = *0.1 m/s. The substrate is preheated to 100°C.*

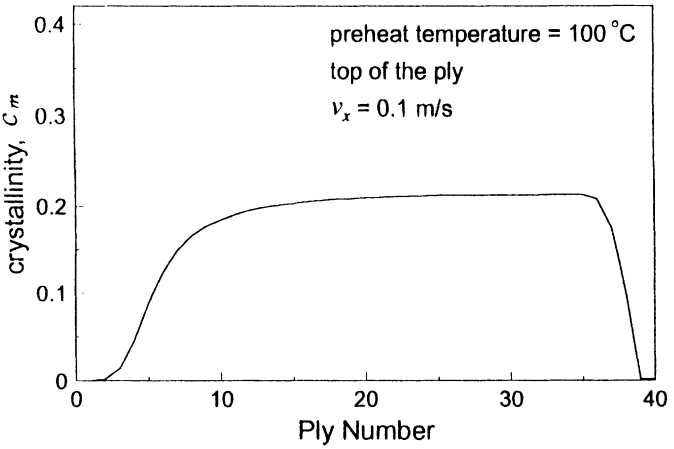

Figure 18. *Final crystallinity levels through the thickness of a 40-ply laminate preheated to 100°C. Roller speed is 0.1 m/s.*

crystallinity to recommended levels. However, choosing a temperature above the glass transition temperature may cause deconsolidation. Therefore, the preheat temperature should be kept close to the glass transition point.

CONCLUSIONS

In this study, heat transfer, crystallization, and degradation models were described, which related the process parameters of tape placement to temperature and crystallinity distribution and degradation weight loss within the composite. In particular, the effects of process parameters on consolidation conditions and crystallization were investigated.

Tape placement is a very complex process with its rapidly changing boundary conditions, incrementally increasing laminate thickness, and large number of process variables. There are no simple rules of thumb to determine the process parameters that are favorable to consolidation. Nevertheless, the following conclusions can be drawn. Consolidation becomes difficult at high speeds due to short dwell times, On the other hand, low laydown speeds are more likely to cause matrix degradation. Preheating of the substrate is advisable. Preheating significantly increases the residence time in the melt due to slower cooling rates. Preheating of the tape or roller, however, does not improve consolidation conditions. Larger heated lengths lead to larger melt zones increasing the residence time. Supplying more heat to the substrate is also beneficial to consolidation. Both the total heated length and the ratio of the heated length on the laminate to the heated length on the tape can be optimized to achieve good bond quality. However, quantifying the effects of process parameters on bonding requires a bonding model, whish is outside the scope of the present study.

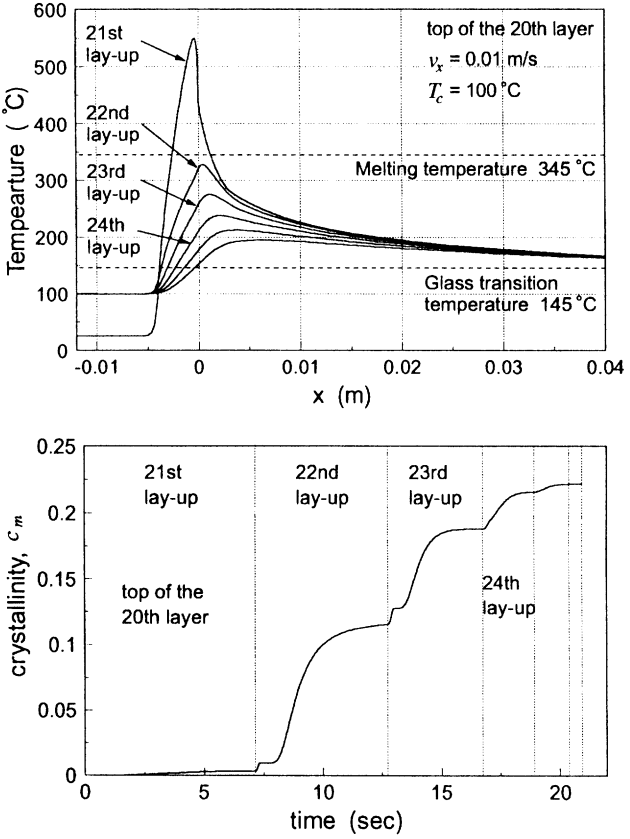

Figure 19. *Temperature profiles and corresponding crystallinity development at the top of the 20th ply during subsequent lay-ups for 0.01 m/s roller speed. The substrate is preheated to 100°C.*

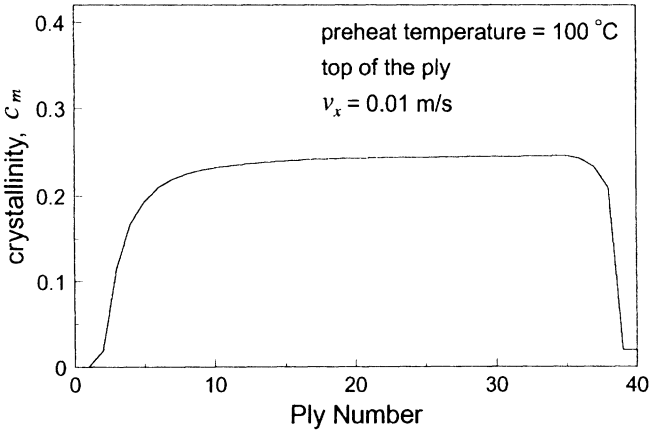

Figure 20. *Final crystallinity levels through the thickness of a 40-ply laminate preheated to 100°C. Roller speed is 0.01 m/s.*

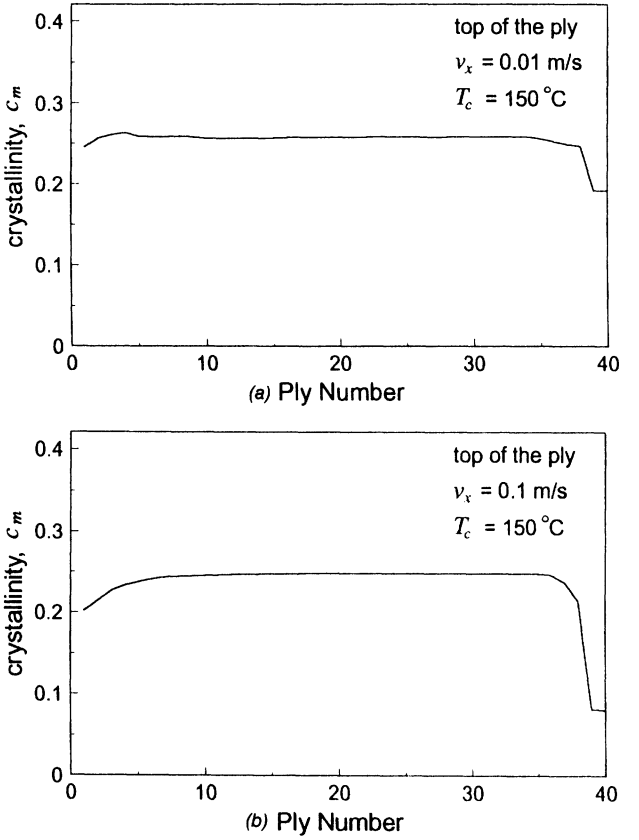

Figure 21. *Final crystallinity level in a 40-ply laminate preheated to 150°C (a)* v_x *= 0.1 m/s, (b)* v_x *= 0.01 m/s.*

Reduced roller speeds resulted in increased crystallinity levels as expected. However, preheating of the substrate was found to be the major factor. Preheating the substrate to a temperature around the glass transition point produced uniform and recommended levels of crystallinity through the thickness of the laminate except for very high speeds.

ACKNOWLEDGEMENT

This paper is based on work supported by The Scientific and Technical Research Council of Turkey (TUBITAK) and also under the Office of Naval Research Grant N00014-92-J-1846 with Dr. Tapa D. S. Rajapakse as the Program Director.

APPENDIX A. FINITE ELEMENT FORMULATION OF THE PROBLEM

Galerkin's method is used to derive a finite element formulation. First, we assume a suitable variation of temperature in a finite element:

$$T(x,y) = \sum_{i=1}^{n} N_i(x,y)T_i = \{N\}^T\{T\}_e \tag{A.1}$$

where $\{T\}_e$ and $\{N\}$ are the vectors of the nodal temperature and shape functions, respectively, and n is the number of nodes in the element. Integrating Equation (8) through the element volume and using the shape functions N_i as weighting factors, for n degrees of freedom for one element, Galerkin method yields

$$\iiint_V N_i\left(k_L\frac{\partial^2 T}{\partial x^2} + k_T\frac{\partial^2 T}{\partial y^2} + \varrho r - \varrho C_p\theta_x\frac{\partial T}{\partial x}\right)dV = 0 \quad i = 1,2,3,\ldots n \tag{A.2}$$

The first term can be expressed as

$$\iiint_V N_i k_L\frac{\partial^2 T}{\partial x^2}\,\mathrm{dV} = \iiint_V k_L\left(\frac{\partial}{\partial x}\left(N_i\frac{\partial T}{\partial x}\right) - \frac{\partial N_i}{\partial x}\frac{\partial T}{\partial x}\right)dV \tag{A.3}$$

Applying Guass's theorem to the first term of the above equation, we get

$$\iiint_V N_i k_L\frac{\partial^2 T}{\partial x^2}\,dV \iint_S N_i k_L\frac{\partial T}{\partial x}n_x dS - \iiint_V k_L\frac{\partial N_i}{\partial x}\frac{\partial T}{\partial x}dV \tag{A.4}$$

After following the same procedure for the second term, Equation (A.1) becomes

$$\iiint_V \left(k_L \frac{\partial N_i}{\partial x}\frac{\partial T}{\partial x} + k_T \frac{\partial N_i}{\partial y}\frac{\partial T}{\partial y} - N_i \varrho r + \varrho C_p v_x N_i \frac{\partial T}{\partial x} \right) dV$$

$$- \iint_S N_i \left(k_L \frac{\partial T}{\partial x} n_x + k_T \frac{\partial T}{\partial y} n_y \right) dS = 0 \qquad \text{(A.5)}$$

The last term vanishes on the boundary A_1, where temperature is specified to be constant because its derivatives with respect to x and y are zero. The last term satisfies heat flux and convection boundary conditions given by Equations (3), (4), (6), and (7). Then

$$\iiint_V \left(k_L \frac{\partial N_i}{\partial x}\frac{\partial T}{\partial x} + k_T \frac{\partial N_i}{\partial y}\frac{\partial T}{\partial y} - N_i \varrho r + N_i \varrho C_p v_x \frac{\partial T}{\partial x} \right) dV$$

$$+ \iint_{A_2} N_i h (T - T_\infty) dA_2 + \iint_{A_3} N_i q dA_3 = 0 \qquad \text{(A.6)}$$

A_1 includes the surfaces S_1 and S_2, A_2 includes the surfaces S_3, S_4, S_5, S_6, S_8 and S_9 (for hot gas heating), and A_3 includes the surface S_9 (for laser heating). If T is replaced by its equivalent given by Equation (A.1), the above equation becomes

$$\sum_{j=1}^{n} \iiint_V \left(k_L \frac{\partial N_i}{\partial x}\frac{\partial N_j}{\partial x} + k_T \frac{\partial N_i}{\partial y}\frac{\partial N_j}{\partial y} + \varrho C_p v_x N_i \frac{\partial N_j}{\partial x} \right) T_j dV - \iiint_V N_i \varrho r dV$$

$$+ \sum_{j=1}^{n} \iint_{A_2} N_i N_j h T_j dA_2 - \iint_{A_2} T_\infty N_i h dA_2$$

$$+ \iint_{A_3} N_i q dA_3 = 0 \qquad i = 1,2,3,\ldots,n \qquad \text{(A.7)}$$

The above equation represents the finite element governing equation, which can be expressed in the following form:

$$[K]_e \{T\}_e = \{P\}_e \qquad \text{(A.8)}$$

where

$$[K]_e = [K'] + [K''] + [K'''] \tag{A.9}$$

$$K'_{ij} = \iiint_V \left(k_L \frac{\partial N_i}{\partial x}\frac{\partial N_j}{\partial x} + k_T \frac{\partial N_i}{\partial y}\frac{\partial N_j}{\partial y} \right) dV \tag{A.10}$$

$$K''_{ij} = \iiint_V \varrho C_p v_x N_i \frac{\partial N_j}{\partial x} dV \tag{A.11}$$

$$K'''_{ij} = \iint_{A_2} N_i N_j h dA_2 \tag{A.12}$$

$$\{P\} = \{P'\} + \{P''\} + \{P'''\} \tag{A.13}$$

$$P'_i = \iint_{A_2} T_\infty N_i h dA_2 \tag{A.14}$$

$$P''_i = -\iint_{A_3} N_i q dA_3 \tag{A.15}$$

$$P'''_i = \iiint_V N_i \varrho r dV \tag{A.16}$$

Here P'''_i accounts for heat generation and release effects during crystallization and melting of crystallites. Substituting Equation (12) into Equation (A.16) and assuming the ratio dc_m/dx is constant within the element, we obtain

$$P'''_i = \varrho m_m H_f v_x \frac{dc_m}{dx} \int_V N_i dV \tag{A.17}$$

P'''_i accounts for heat generation and release effects during crystallization and melting of crystallites.

The temperature variation inside the element is assumed to be in bilinear form.

$$T = a_1 + a_2 x + a_3 y + a_4 xy \tag{A.18}$$

Solving the a's in terms of nodal temperatures allows us to obtain shape functions $\{N\}$ in Equation (A.1). Then, Equation (A.10) through Equation (A.17) can

be calculated to obtain $[K]_e$ and $\{P\}_e$ [115]. In particular, Equation (A.17) becomes

$$\{P'''\} = \varrho m_m H_f v_x \frac{dc_m}{dx} \frac{ab}{4} \{1 \quad 1 \quad 1 \quad 1\} \tag{A.19}$$

When $[K]_e$ and $\{P\}_e$ are calculated for each rectangular element, the second and third types of boundary conditions (convection on A_2 and heat flux A_3) are already incorporated into the finite element governing equation, Equation (A.8). By following standard procedures [116,117], they are then assembled to obtain the global equation:

$$[K]\{T\} = \{P\} \tag{A.20}$$

where $[K]$ is the global matrix having a dimension of $(m \times m)$, m being the total number of nodes in the mesh structure, $\{T\}$ is the vector of nodal temperatures with a dimension of $(m \times 1)$, and $\{P\}$ is the global force vector. The global matrix is not symmetric due to the heat transport component, $[K'']$.

Considering that $[K]$ is a singular matrix, the above equation cannot be solved without incorporating first type boundary conditions. The boundary conditions on A_1, where temperature is specified, are introduced by reducing the global matrix and the global force vector to their unspecified degrees of freedom.

$$\begin{bmatrix} K_{uu} & K_{us} \\ K_{su} & K_{ss} \end{bmatrix} \begin{Bmatrix} T_u \\ T_s \end{Bmatrix} = \begin{Bmatrix} P_u \\ P_s \end{Bmatrix} \tag{A.21}$$

where $\{T_u\}$ is the vector of unspecified node temperatures, and $\{T_s\}$ is the vector of specified node temperatures. Then, unknown node temperatures are given by

$$\{T_u\} = [K_{uu}]^{-1}(\{P_u\} - [K_{us}]\{T_s\}) \tag{A.22}$$

REFERENCES

1. Lee, I. L. and G. S. Springer. 1987. "A Model of the Manufacturing Process of Thermoplastic Matrix Composites," *Journal of Composite Materials,* 21:1017–1055.
2. Velisaris, C. N. and J. C. Seferis. 1988. "Heat Transfer Effects on the Processing-Structure Relationship of Polyetheretherketone (PEEK) Based Composites," *Polymer Engineering and Science,* 28(9):583–591.
3. Blundell, D. J. and F. M. Willmouth. 1986. "Crystalline Morphology of the Matrix of PEEK-Carbon Fiber Aromatic Polymer Composites," *SAMPE Quarterly,* 17(2):50–57.
4. Hwang, S. J. and C. L. Tucker. 1990. "Heat Transfer Analysis of Continuous Fiber/Thermoplastic Matrix Composites during Manufacture," *Journal of Thermoplastic Composite Materials,* 3:441–51.
5. Saliba, T. E., D. P. Anderson and R. A. Servais. 1989. "Process Modeling of Heat Transfer and Crystallization in Complex Shape Thermoplastic Composites," *Journal of Thermoplastic Composite Materials,* 2:91–103.

6. Maffezzoli, A. M., J. M. Kenny and L. Nicolais. 1989. "Welding of PEEK/Carbon Fiber Composite Laminates," *SAMPE Journal,* 25(1):35–39.
7. Maffezzoli, A. M., J. M. Kenny and L. Nicolais. 1989. "Modeling of Thermal and Crystallization Behavior of the Processing of Thermoplastic Matrix Composites," *Materials and Processing—Move into 90's,* pp. 133–143.
8. Xiao, X. R., S. V. Hoa and K. N. Street. 1992. "Processing and Modeling of Resistance Welding of APC-2 Composites," *Journal of Composite Materials,* 26(7):1031–1049.
9. Beyeler, E. P. and S. I. Guyceri. 1988. "Thermal Analysis of Laser Assisted Thermoplastic-Matrix Composite Tape Consolidation," *Journal of Heat Transfer,* 110:424–430.
10. Astrom, B. T. and R. B. Pipes. 1993. "A Modeling Approach to Thermoplastic Pultrusion. I-Formulation of Models," *Polymer Composites,* 14(3):173–183.
11. Grove, S. M. 1988. "Thermal Modeling of Tape Laying with Continuous Carbon-Fiber-Reinforced Thermoplastics," *Composites,* 19:367–375.
12. Nejhad, M. N. G., R. D. Cope and S. I. Guceri. 1991. "Thermal Analysis of In-Situ Thermoplastic Composite Tape Laying," *Journal of Thermoplastic Composite Materials,* 4:20–45.
13. Mantell, S. C. and G. S. Springer. 1992. "Manufacturing Process Models for Thermoplastic Composites," *Journal of Composite Materials,* 26(16):2348–2377.
14. Nejhad, M. N. G. 1993. "Issues Related to Processability during the Manufacture of Thermoplastic Composites Using On-Line Consolidation Techniques," *Journal of Thermoplastic Composite Materials,* 6:130–145.
15. Pitchumani, R., R. C. Don, J. W. Gillespie and S. Ranganathan. 1994. "Analysis of On-Line Consolidation during Thermoplastic Tow-Placement Process," in *Thermal Processing of Materials: Thermo-Mechanics, Controls and Composites (ASME),* HTD, 289:223–234.
16. Sarrazin, H. and G. S. Springer. 1994. "Thermochemical and Mechanical Aspects of Composite Tape Laying," *Journal of Composite Materials,* 29(14):1908–1943.
17. Brage, A. and C. Lamrell. 1988. "Heat Flow Analysis in Connection with Thermoplastic Filament Winding," *SAMPE Quarterly,* 19(3):31–35.
18. James, D. L. and W. Z. Black. 1994. "Experimental Analysis and Process Window Development for Continuous Filament Wound APC-2," in *Thermal Processing of Materials: Thermo-Mechanics, Controls and Composites (ASME),* HTD, 289:203–212.
19. Nejhad, M. N. G., R. D. Cope and S. I. Guceri. 1991. "Thermal Analysis of In-Situ Thermoplastic-Matrix Composite Filament Winding," *Transactions of ASME,* 113:304–313.
20. Gruber, M. B. "Thermoplastic Tape Laydown and Consolidation," *SME Technical Paper,* EM86-905, pp. 1–15.
21. Curry, W. R. 1986. "Flat Thermoplastic Tape Laying," *2nd ASM Conference on Advanced Composites,* Dearborn, Michigan, pp. 45–50.
22. Anderson, B. J. and J. S. Colton. 1989. "A Study in the Lay-Up and Consolidation of High Performance Thermoplastic Composites," *Tomorrow's Materials: Today,* Society for the Advancement of Material and Process Engineering, 24:1952–1963.
23. Grove, S. M. and D. Short. 1988. "Evaluation of Carbon Fibre-Reinforced PEEK Composites Manufactured by Continous Local Welding of Prepreg Tape," *Plastics and Rubber Processing and Applications,* 10:1.
24. Mantell, S., Q. Wang and G. S. Springer. 1992. "Processing Thermoplastic Composites in a Press and by Tape Laying—Experimental Results," *Journal of Composite Materials,* 26:2378–24301.
25. Hinkley, J. A. R. W. Grenoble and J. M. Marchello. 1995. "Rapid Welding of Thermoplastic Towpreg Ribbon, *40th International SAMPE Symposium,* 1560–1571.
26. Wood, D. and S. C. Mantell. 1993. "Application of Statistical Design of Experiments to Thermoplastic Tape Laying," *38th International SAMPE Symposium, pp. 152–162.*
27. Beyeler, E., W. Phillips and S. I. Guceri. 1988. "Experimental Investigation of Laser-Assisted Thermoplastic Tape Consolidation," *Journal of Thermoplastic Composite Materials,* 1:107–121.

28. Fedro, M. J., D. W. Jensen and H. T. Hah. "Filament Winding of Thermoplastic Composites Using Commingled Yarns," *SME Technical Paper,* EM89-584, pp. 1-18.
29. Rowan, J. H. C. and R. N. Askander. 1989. "Filament Winding of High Performance Thermoplastic Composites," *Materials and Processing-Move into 90's,* Elsevier, pp. 11-20.
30. Werdermann, C., K. Friedrich, M. Cirino and R. B. Pipes. 1989. "Design and Fabrication of an On-Line Consolidation Facility for Thermoplastic Composites," *Journal of Thermoplastic Composite Materials,* 2:293-306.
31. Astrom, B. T. and R. B. Pipes. 1990. "Thermoplastic Filament Winding with On-Line Impregnation," *Journal of Thermoplastic Composite Materials,* 3:314-324.
32. Hardtmann, D. and Bubeck, K. 1990. "Technical Evaluation of *ROWS* Thermoplastic Composite Fiber Placement System," *22nd International SAMPE Technical Conference,* pp. 1092-1105.
33. Enders, M. L. 1990. "Developments in Thermoplastic Filament Winding," *22nd International SAMPE Technical Conference,* pp. 88-97.
34. Roychowdhury, S. and S. G. Advani. 1991. "An Experimental Investigation of Consolidation in Thermoplastic Filament Winding," *Composite Manufacturing,* 2(2):97-104.
35. Colton, J. A. and D. Leach. 1991. "Processing Parameters for Thermoplastic Filament Winding," *Processing and Manufacturing of Composite Materials-ASME,* PED-Vol. 49/MD-Vol. 27, pp. 231-245.
36. Hummler, J., S.-K. Lee and K. V. Steiner. 1991. "Recent Advances in Thermoplastic Robotic Filament Winding," *36th International SAMPE Symposium,* pp. 2142-2156.
37. Cirino, M., T. P. Watson and D. W. Hauber. 1991. "Composite Structure Fabrication, with In-Situ Consolidation of APC-2/AS4," *36th International SAMPE Symposium,* pp. 2184-2196.
38. Felderhoff, K. D. and K. V. Steiner. 1993. "A New Compact Robotic Head for Thermoplastic Fiber Placement," *38th International SAMPE Symposium,* pp. 138-151.
39. Mazumdar, S. K. and S. V. Hoa. 1993. "Processing of PEEK/Carbon Thermoplastic Composites Using Hot Nitrogen Gas by Tape Winding Technique," *Heat and Mass Transfer in Materials Processing and Manufacturing-ASME,* HTD-Vol. 261, pp. 115-126.
40. Carpenter, C. E. and J. S. Colton. 1994. "On-Line Consolidation Mechanisms in Thermoplastic Filament Winding," *Polymer Composites,* 15(1):55-63.
41. Agarwal, V., S. I. Guceri, R. L. McCullough and J. M. Schultz. 1992. "Thermal Characterization of the Laser Assisted Consolidation Process," *Journal of Thermoplastic Composite Materials,* 115-135.
42. Wagner, P. and J. Colton. 1994. "On-Line Consolidation of Thermoplastic Towpreg Composites in Filament Winding," *Polymer Composites,* 15(6):436-441.
43. Mazumdar, S. K. and S. V. Hoa. 1993. "Experimental Determination of Process Parameters for Laser Assisted Processing of PEEK/Carbon Thermoplastic Composites," *38th International SAMPE Symposium,* pp. 189-204.
44. Steiner, K. V., B. M. Bauer, R. Pitchumani and J. W. Gillespie. 1995. "Experimental Verification of Modeling and Control for Thermoplastic Tow Placement," *40th International SAMPE Symposium,* pp. 1550-1559.
45. Sandusky, D. A., J. M. Marchello, R. M. Baucom and N. J. Johnston. 1992. "Customized ATP Towpreg," *24th International SAMPE Technical Conference,* pp. T591-T605.
46. Mazumdar, S. K. and S. V. Hoa. 1995. "Application of Taguchi Method for Process Enhancement of On-Line Consolidation Technique," *Composites,* 26:669-673.
47. Sandusky, D. A. J. M. Marchello, R. M. Baucom and N. J. Johnston. 1992. "Customized ATP Towpreg," *24th International SAMPE Technical Conference,* pp. T591-T605.
48. Cogwell, F. N. 1992. "Thermoplastic Aromatic Polymer Composites," Butterworth-Heinemann Ltd.
49. Scobbo, J. J. and N. Nakajima. "Time-Temperature Processing Windows for Thermoplastic/Graphite Fiber Composites," *ANTEC '90,* pp. 1397-1400.

50. Moddeman, W. E., W. C. Bowling, E. E. Tibbetts and R. B. Whitaker. 1986. "Thermal Stability and Compatibility of Polyetheretherketone (PEEK) with an Oxidizer and Pyrotechnic Blend," *Polymer Engineering and Science,* 26(21):1469–1477.

51. Prime, R. B. and J. C. Seferis. 1986. "Thermo-Oxidative Decomposition of Poly (Ether Ether Ketone)," *Journal of Polymer Science: Part C: Polymer Letters,* 234:641–644.

52. Hay, J. N. and D. J. Kemmish. 1987. "Thermal Decomposition of Poly (Aryl Ether Ether Ketone)," *Polymer,* 28:2047–2051.

53. Day, M., J. D. Cooney and D. M. Wiles. 1990. "The Thermal Degradation of Poly(Aryl-Ether-Ether-Ketone) (PEEK) as Monitored by Pyrolysis-Gc/Ms and Tg/Ms," *Journal of Analytical and Applied Pyrolysis,* 18(2):163–173.

54. Day, M., J. D. Cooney and D. M. Wiles. 1989. "A Kinetic Study of the Thermal Decomposition of Poly(Aryl-Ether-Ether-Ketone) (PEEK) in Nitrogen," *Polymer Engineering and Science,* 29(1):19–22.

55. Day, M., J. D. Cooney and D. M. Wiles. 1989. "The Thermal Stability of Poly(Aryl-Ether-Ether-Ketone) as Assessed by Thermogravimetry," *Journal of Applied Polymer Science,* 38:323–337.

56. Day, M., J. D. Cooney and D. M. Wiles. 1989. "The Kinetics of the Oxidative Degradation of Poly(Aryl-Ether-Ether-Ketone) (PEEK), *Thermochimica Acta,* 147(1):189–187.

57. Day, M., D. Sally and D. M. Wiles. 1990. "Thermal Degradation of Poly(Aryl-Ether-Ether-Ketone)-Experimental Evaluation of Crosslinking Reactions," *Journal of Applied Polymer Science,* 40:1615–1625.

58. Nam, J.-D. and J. C. Seferis. 1992. "Generalized Composite Degradation Kinetics for Polymeric Systems under Isothermal and Nonisothermal Conditions," *Journal of Polymer Science: Part B (Polymer Physics),* 30(5):455–463.

59. Carpenter, J. F. 1988. "Thermal Analysis and Crystallization Kinetics of High-Temperature Thermoplastics," *SAMPE Journal,* 24:36–39.

60. Jonas, A. and R. Legras. 1993. "PEEK Degradation and Its Influence on Crystallization Kinetics," in *Advanced Thermoplastic Composites-Characterizing Processing,* Hanser, pp. 57–81.

61. Corrigan, E., D. Leach and T. McDaniels. 1989. "The Influence of Processing Conditions on the Properties of PEEK Matrix Composites," *Materials and Processing-Move into 90's,* pp. 121–131.

62. Davies, P., W. J. Cantwell, P. Y. Jar, H. Richard, D. J. Neville and H. Kausch. 1991. "Cooling Rate Effects in Carbon Fiber/PEEK Composites," *Composite Materials: Fatigue and Fracture,* Third Volume, ASTM STP 110:70–88.

63. Grossman, S. and M. F. Ameteau. 1988. "The Effect of Processing on a Graphite Fiber/Polyetheretherketone Thermoplastic Composite," *Proceedings of 33rd SAMPE Symposium,* pp. 681–692.

64. Curtis, P. T., P. Davies, I. K. Partridge and J. P. Sainty. 1987. "Cooling Rate Effects in PEEK and Carbon Fiber-PEEK Composites," *Proceedings of 6th International Conference on Composite Materials,* pp. 4.401–4.412.

65. Folkes, J. J., G. Kalay and A. Ankara. 1993. "The Effect of Heat Treatment on the Properties of PEEK and APC-2," *Composites Science and Technology,* 46:77–83.

66. Xiao, X. R., J. Denault and T. Vu-Khanh. 1992. "The Effect of Low Melt Temperature on Morphology and Mode-I Fracture Toughness of PEEK/Carbon Composite," *Journal of Thermoplastic Composite Materials,* 5:64–75.

67. Cantwell, W. J. P. Davies and H. H. Kausch. 1990. "The Effect of Cooling Rate on Deformation and Fracture of IM6/PEEK Composites," *Composite Structures,* 14:151–171.

68. Tregub, A., H. Harel and G. Marom. 1993. "The Influence of the Thermal History on the Mechanical Properties of Poly(Ether Ether Ketone) Matrix Composite Materials," *Composite Science and Technology,* 48:185–190.

69. Saib, K. S., W. J. Evans and D. H. Isaac. 1993. "The Role of Microstructure during Fatigue Crack Growth in Poly(aryl ether ether ketone) (PEEK)," *Polymer,* 34(15):3199–3203.

70. Talbott, M. F., G. S. Springer and L. A. Burglund. 1987. "The Effects of Crystallization on the Mechanical Properties of PEEK Polymer and Graphite Fiber Reinforced PEEK," *Journal of Composite Materials,* 21:1056–1081.

71. Cantwell, W. J. and H. H. Kausch. 1992. "An Evaluation of the Interlaminar Fracture Toughness of a Thermoplastic Composite with Offset Center Flies," *Mekhanika Kompozitnykh Materialov,* 4:476–483.

72. Lustiger, A., F. S. Uralil and G. M. Newaz. 1990. "Processing and Structural Optimization of PEEK Composites," *Polymer Composites,* 11:65–75.

73. Cebe, P., S. Y. Chung and S.-D. Hong. 1987. "Effect of Thermal History on Mechanical Properties of Polyetheretherketone below the Glass Transition Temperature," *Journal of Applied Polymer Science,* 33:487–503.

74. Tung, C. M. and P. J. Dynes. 1987. "Morphological Characterization of Poly Ether Ether Ketone-Carbon Fiber Composites," *Journal of Applied Polymer Science,* 33:505–520.

75. D'Amore, A. and L. Nicolais. 1992. "The Effect of Fibre and Crystallinity Content on the Structural Relaxation of Polyetheretherketone (PEEK)," *Composites Manufacturing,* 3:25–31.

76. Lawrence, W. E., J. C. Seferis and J. W. Gillespie. 1992. "Material Response of a Semicrystalline Thermoplastic Polymer and Composite in Relation to Process Cooling History," *Polymer Composites,* 13(2):86–96.

77. Sichina, W. and P. S. Gill. 1988. "Characterization of Composites Using Dynamic Mechanical Analysis," *33rd International SAMPE Symposium,* pp. 1–11.

78. Stober, E. J., J. C. Seferis and J. D. Keenan. 1984. "Characterization and Exposure of Polyetheretherketone (PEEK) to Fluid Environments," *Polymer,* 25:1845–1852.

79. Unger, W. J. and J. S. Hansen. 1993. "The Effect of Cooling Rate and Annealing on Residual Stress Development in Graphite Fibre Reinforced PEEK Laminates," *Journal of Composite Materials,* 27(2):108–135.

80. Avrami, M. 1939. "Kinetics of Phase Change I, General Theory," *Journal of Chemical Physics,* 7:1103–1112.

81. Avrami, M. 1940. "Kinetics of Phase Change II, Transformation-Time Relations for Random Distribution of Nuclei," *Journal of Chemical Physics,* 8:212–224.

82. Avrami, M. 1941. "Kinetics of Phase Change. III, Granulation, Phase Change and Microstructure," *Journal of Chemical Physics,* 9:177–184.

83. Tobin, M. C. 1974. "Theory of Phase Transition Kinetics with Growth Site Impingement. I. Homogeneous Nucleation," *Journal of Polymer Science: Polymer Physics Edition,* 12:399–406.

84. Tobin, M. C. "The Theory of Phase Transition Kinetics with Growth Site Impingement. II. Heterogeneous Nucleation," *Journal of Polymer Science: Polymer Physics Edition,* 14:2253–2257.

85. Tobin, M. C. 1977. "Theory of Phase Transition Kinetics with Growth Site Impingement. III. Mixed Heterogeneous-Homogeneous Nucleation and Noninternal Exponents of the Time," *Journal of Polymer Science: Polymer Physics Edition,* 15:2269–2270.

86. Malin, A. Y., V. P. Beghishev. I. A. Keapin and S. A. Bolgov. 1984. "General Treatment of Polymer Crystallization Kinetics-Part 1. A New Macrokinetic Equation and its Experimental Verification," *Polymer Engineering and Science,* 24(18):1396–1401.

87. Malkin, A. Y., V. P. Beghishev, I. A. Keapin and Z. P. Andrianova. 1984. "General Treatment of Polymer Crystallization Kinetics-Part 2. The Kinetics of Nonisothermal Crystallization," *Polymer Engineering and Science,* 24(18):1402–1408.

88. Valisaris, C. N. and J. C. Seferis. 1986. "Crystallization Kinetics of Polyetheretherketone (PEEK) Matrices," *Polymer Engineering and Science,* 26(22):1574–1581.

89. Seferis, J. C., C. Ahlstrom and S. H. Dillman. 1987. "Cooling Rate and Annealing as Pro-

cessing Parameters for Semicrystalline Thermoplastic Based Composites," *ANTEC,* pp. 1467–1471.

90. Patel, R. M. and J. E. Spruiell. 1991. "Crystallization Kinetics During Polymer Processing-Analysis of Available Approaches for Process Modeling," *Polymer Engineering and Science,* 31(10):730–738.
91. Cebe, P. 1988. "Application of Parallel Avrami Model to Crystallization of Poly(Etheretherketone)," *Polymer Engineering and Science,* 28(18):1192–1197.
92. Cebe, P. 1988. "Non-Isothermal Crystallization of Poly(Etheretherketone) Aromatic Polymer Composite," *Polymer Composites,* 9(4):271–279.
93. Cebe, P. and S.-D. Hong. "Crystallization Behavior of Poly(Ether-Ether-Ketone)," *Polymer,* 27:1183–1192.
94. Choe, C. R. and K. H. Lee. 1989. "Nonisothermal Crystallization Kinetics of Poly (Etheretherketone) (PEEK)," *Polymer Engineering and Science,* 29(12):801–805.
95. Blundell, D. J. and B. N. Osborn. 1985. "Crystalline Morphology of the Matrix of PEEK-Carbon Fiber Aromatic Polymer Composites, II. Crystallizaton Behaviour," *SAMPE Quarterly,* 17(1):1–16.
96. Tai, H.-J., W.-Y. Chiu, L.-W. Chen and L.-H. Chu. 1991. "Study of Crystallization Kinetics of PP/GF Composites," *Journal of Applied Polymer Science,* 42:3111–3122.
97. Nakamura, K. K. Katayama and T. Amano. 1973. "Some Aspects of Nonisothermal Crystallization of Polymers. II. Consideration of the Isokinetic Condition," *Journal of Applied Polynmer Science,* 17:1031–1041.
98. Ozaza, T. 1971. "Kinetics of Nonisothermal Crystallization," *Polymer,* 12:150–158.
99. Kamal, M. R. and E. Chu. 1983. "Isothermal and Nonisothermal Crystallization of Polyethylene," *Polymer Engineering and Science,* 23(1):27–31.
100. Kenny, J. M., A. Maffezzoli, and L. Nicolais. 1993. "A New Kinetic Model for Polymer Crystallization Derived by Calorimetic Analysis," *Thermochimica Acta,* 227:83–95.
101. Lee, K. H. and S. C. Kim. "Reaction-Induced Crystallization Kinetics during the Anionic Polymerizaton of ϵ-Caprolactam," *Polymer Engineering and Science,* 28(1):13–19.
102. Eder, G., H. Kaneschitzkriegl and S. Liedauer. 1990. "Crystallization Process in Quiescent and Moving Polymer Melts under Heat Transfer Conditions," *Progress in Polymer Science,* 15(4):629–714.
103. Blundell, D. J., R. A. Crick, B. Fife, J. Peacock and A. Keller. 1989. "Spherulitic Morphology of the Matrix of Thermoplastic PEEK/Carbon Fiber Aromatic Polymer Composites," *Journal of Material Science,* 24:2057–2064.
104. Blundell, D. J. and B. N. Osborn. 1983. "The Morphology of Poly(Aryl-Ether-Ether-Ketone)," *Polymer,* 24:953–958.
105. Kumar, S. and D. P. Anderson. 1986. 1986. "Crystallization and Morphology of Poly(Aryl-Ether-Ether-Ketone)," *Polymer,* 27:329–336.
106. Deslandes, Y., M. Day, N. F. Sbir and T. Suprunchuk. 1989. "Crystallization of Poly(Aryl-Ether-Ether-Ketone): Effect of Thermal History of the Melt on Crystallization Kinetics," *Polymer Composites,* 10:360–366.
107. Nejhad, M. N. G., J. W. Gillespie and R. D. Cope Jr. 1992. "Prediction of Process-Induced Stresses for In-Situ Thermoplastic Filament Winding of Cylinders," Proceedings of 3rd International Conference, *Computer Aided Design in Composite Material Technolgy,* Newark, Delaware, Vol. 3, pp. 277–295.
108. Rodkey, R. S. and H. C. Hershey. "Transport Phenomena," McGraw-Hill, 1988.
109. Mandelkern, L. 1964. "Crystallization of Polymers," McGraw Hill, New York.
110. Cormia, R. L., F. P. Price and D. Turnbull. 1962. "Kinetics of Crystal Nucleation in Polyethylene," *The Journal of Chemical Physics,* 37(6):1333–1340.
111. Blundell, D. J., J. M. Chalmes, MacKenzie and W. F. Gaskkin. 1985. "Crystalline Morphology

of the Matrix of PEEK-Carbon Fiber Aromatic Polymer Composites, I. Assessment of Crystallinity," *SAMPE Quarterly,* 16(4):22–30

112. Kenny, J., A. D'Amore and L. Nicolais. 1989. "Processing of Amorphous PEEK and Amorphous PEEK Based Composites," *SAMPE Journal,* 25:27–34.
113. Konnecke, K. 1994. "Crystallization of Poly(Aryl Ether Ketones). I. Crystallization Kinetics," *Journal of Macromolecular Science-Physics,* B33(1):37–62.
114. Geankoplis, C. J. 1983. "Transport Process and Unit Operations," Allyn and Bacon Inc.
115. Sonmez, F. O. 1995. "Modeling of the Thermoplastic Composite Tape Placement Process," Ph.D. thesis, UCLA, Los Angeles, 1995.
116. Yang, T. Y. 1986. "Finite Element Structural Analysis," Prentice-Hall.
117. Rao, S. S. 1989. "The Finite Element Method in Engineering," Pergamon Press.